## ORIGINAL RESEARCH

Myeloid Cell-Derived HB-EGF Drives Tissue Recovery After Pancreatitis

Hui-Ju Wen,[1] Shan Gao,[2] Yin Wang,[3] Michael Ray,[4] Mark A. Magnuson,[5] Christopher V. E. Wright,[4] Marina Pasca Di Magliano,[6,7,8] Timothy L. Frankel,[6] and Howard C. Crawford[1,3,7]

[1]Department of Molecular and Integrative Physiology, [3]Department of Internal Medicine, [6]Department of Surgery, [7]Rogel Comprehensive Cancer Center, [8]Department of Cell and Developmental Biology, University of Michigan, Ann Arbor, Michigan; [2]Department of Gastroenterology, The Second Xiangya Hospital, Central South University, China; [4]Department of Cell and Developmental Biology, [5]Department of Molecular Physiology and Biophysics, Center for Stem Cell Biology, Vanderbilt University, Nashville, Tennessee
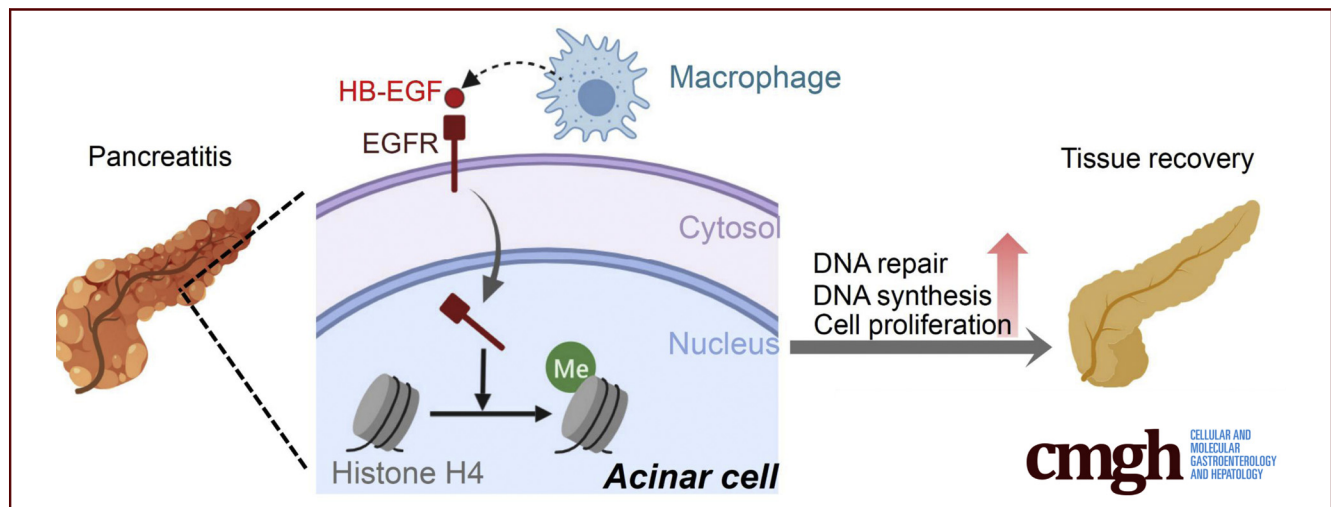
SUMMARY

Macrophages play a critical role in pancreatitis progression and pancreas regeneration. Heparin-binding epidermal growth factor receptor–like growth factor derived from myeloid cells is not involved in the initiation of pancreatitis, but contributes to pancreas recovery after pancreatitis by promoting DNA damage repair.

BACKGROUND & AIMS: Pancreatitis is a major cause of morbidity and mortality and is a risk factor for pancreatic tumorigenesis. Upon tissue damage, an inflammatory response, made up largely of macrophages, provides multiple growth factors that promote repair. Here, we examine the molecular pathways initiated by macrophages to promote pancreas recovery from pancreatitis.

METHODS: To induce organ damage, mice were subjected to cerulein-induced experimental pancreatitis and analyzed at various times of recovery. *CD11b-DTR* mice were used to deplete myeloid cells. *Hbegf$^{f/f}$;LysM-Cre* mice were used to ablate myeloid cell–derived heparin-binding epidermal growth factor (EGF)-like growth factor (HB-EGF). To ablate EGFR specifically during recovery, pancreatitis was induced in *Egfr$^{f/f}$;Ptf1a$^{FlpO/+}$;FSF-Rosa26$^{CAG-CreERT2}$* mice followed by tamoxifen treatment.

RESULTS: Macrophages infiltrating the pancreas in experimental pancreatitis make high levels of HB-EGF. Both depletion of myeloid cells and ablation of myeloid cell HB-EGF delayed recovery from experimental pancreatitis, resulting from a decrease in cell proliferation and an increase in apoptosis. Mechanistically, ablation of myeloid cell HB-EGF impaired epithelial cell DNA repair, ultimately leading to cell death. Soluble HB-EGF induced EGFR nuclear translocation and methylation of histone H4, facilitating resolution of DNA damage in pancreatic acinar cells in vitro. Consistent with its role as the primary receptor of HB-EGF, in vivo ablation of EGFR from pancreatic epithelium during recovery from pancreatitis resulted in accumulation of DNA damage.

CONCLUSIONS: By using novel conditional knockout mouse models, we determined that HB-EGF derived exclusively from myeloid cells induces epithelial cell proliferation and EGFR-dependent DNA repair, facilitating pancreas healing after injury. *(Cell Mol Gastroenterol Hepatol 2019;8:173–192;* https://doi.org/10.1016/j.jcmgh.2019.05.006*)*

Keywords: DNA Damage; EGFR; Inflammation; Macrophages.

Pancreatitis is a type of tissue injury commonly associated with heavy alcohol consumption, smoking, and ductal blockage by gallstones. Although acute pancreatitis can be mild and self-resolving, at its most severe it can be a necrotizing disease leading to endocrine and/or exocrine impairment and even multiple organ dysfunction. Repeated bouts of acute pancreatitis also can become fibrotic chronic pancreatitis, a risk factor for pancreatic cancer.[1] Pancreatitis is the most frequent cause of hospitalization in gastrointestinal diseases.[2,3] During pancreatitis, acinar cell dropout results from apoptosis, necrosis, and necroptosis,[4] while some acinar cells undergo transdifferentiation to ductal structures in a process known as acinar-to-ductal metaplasia (ADM).[5–7] ADM can act as a precursor of neoplasia upon oncogenic mutation of Kras,[8,9] which can progress to pancreatic cancer. In cerulein-induced experimental pancreatitis in mice, ADM is a cell survival mechanism in the face of abundant tissue damage and cell death. Upon injury resolution, metaplastic epithelia can redifferentiate back to acinar cells, restoring homeostasis.[10,11]

One of the hallmarks of pancreatitis is an influx of innate immune cells, including a large number of macrophages.[12,13] Numerous experimental and clinical studies have indicated that proinflammatory mediators (eg, tumor necrosis factor [TNF-α], interleukin [IL]6, IL8, and so forth) released from acinar cells induce macrophage infiltration, which supports the progression of pancreatitis.[14–18] Macrophages contribute to the pancreatitis phenotype by inducing ADM and fibrogenesis.[18,19] Conversely, macrophages are important for tissue regeneration under conditions in which most of the pancreatic epithelial cells are ablated,[20] suggesting that they produce factors that promote cell proliferation and differentiation after severe injury.

Heparin-binding epidermal growth factor–like growth factor (HB-EGF) initially was identified in conditioned medium of cultured human macrophages,[21] and is highly expressed in macrophages associated with human pancreatic cancer and chronic pancreatitis.[22] HB-EGF is synthesized as a transmembrane protein and shed by a disintegrin and metalloproteinases (ADAMs) to become a soluble growth factor, capable of binding to the receptors EGF receptor (EGFR) and Receptor tyrosine-protein kinase erbB-4 (ERBB4).[23] The transmembrane precursor of HB-EGF is also biologically active and can signal in a juxtacrine fashion to adjacent cells.[24] HB-EGF binding to EGFR/ERBB4 activates downstream signaling cascades that are associated with cell survival, proliferation, and migration. Indeed, ectopic HB-EGF promotes keratinocyte migration in skin wound healing.[25,26] Together with its function in other types of wound repair, we hypothesized that macrophage-derived HB-EGF plays an important role in pancreas recovery after pancreatitis-associated injury.

In the current study, we genetically ablated HB-EGF exclusively from myeloid cells to definitively determine its contribution to pancreas wound healing. In a model of severe acute experimental pancreatitis, ablation of myeloid HB-EGF had no significant effect on ADM induction or inflammatory cell infiltration, but drastically inhibited tissue repair, phenocopying the effects of widespread ablation of myeloid cells during this recovery phase. HB-EGF ablation from myeloid cells decreased epithelial cell proliferation, enhanced cell death, and slowed DNA repair, effects that manifested after cessation of cerulein-induced injury. We found that HB-EGF enhanced DNA repair through induction of EGFR nuclear localization and histone H4 methylation. Our findings clearly show that myeloid-derived HB-EGF is uniquely required for epithelial cell DNA repair and tissue restoration after pancreatic injury in vivo.

Results

Myeloid Cells Are Required for Tissue Recovery After Experimental Pancreatitis

Macrophages are required for pancreatic cell regeneration after mass ablation of pancreatic epithelia,[20] leading us to investigate whether myeloid cells similarly contribute to organ recovery from a milder form of injury more similar to human pancreatitis. To test this, we used transgenic mice expressing diphtheria toxin receptor (DTR) under the control of the myeloid-specific CD11b promoter (CD11b-DTR), allowing us to deplete CD11b$^+$ myeloid cells by administering DT.[27] To induce injury, we repeated cerulein injections twice daily for 2 weeks, and harvested pancreata 1 and 7 days later (Figure 1A).[28] Two weeks of cerulein treatment resulted in a severe form of acute pancreatitis including tissue atrophy and ADM, accompanied by macrophage infiltration (Figure 1B). With 7 days of recovery, the number of macrophages decreased and repopulation of acinar cells was evident by an increase in amylase-positive cells and a decrease in Cytokeratin 19 (CK19)-positive ductal cells (Figure 1Ca–d). Strikingly, depletion of myeloid cells throughout the 7-day recovery period prevented restoration of the acinar cell compartment (Figure 1Ce–h) but did not affect relative pancreatic mass (Figure 1D). All pancreata showed numerous Ki67$^+$ cells, with the majority being acinar cells in saline-treated controls (Figure 1E and Fa, arrows), but limited to the interstitial space in DT-treated mice (Figure 1E and Fb, arrowheads). The lack of acinar cell proliferation in DT-treated mice was accompanied by a significantly higher number of cleaved caspase-3$^+$ apoptotic cells compared with saline-treated controls (Figure 1G and H). Thus, consistent with other injury models,

Figure 1. Depletion of myeloid cells impairs pancreatic recovery from experimental pancreatitis. (*A*) Schematic of cerulein treatment protocol for *CD11b-DTR* mice. (*B* and *C*) H&E staining and IHC for amylase, CK19, and F4/80 on pancreas sections from *CD11b-DTR* mice treated with cerulein for 2 weeks followed by (*B*) 1-day recovery (1dR) and (*C*) 7-day recovery (7dR). *Scale bar*: 100 μm. Quantitation of IHC for amylase, CK19, and F4/80 on pancreata from saline and DT-treated mice (n = 3). (*D*) Analysis of pancreas-to-body weight ratios (PW/BW) of *CD11b-DTR* mice with saline or DT treatment (n = 6). (*E* and *G*) IHC for Ki67 and CC3 on pancreata after 7-day recovery. *Scale bar*: 20 μm. Quantitation of IHC for Ki67-positive (n = 4) and CC3-positive (n ≥ 4) epithelial cells. (*F* and *H*) Representative immunofluorescent images for E-cadherin (E-cad) (green), Hoechst33342 (blue), and (*F*) Ki67 or (*H*) CC3 (red) on 7-day recovery pancreata from CD11b-DTR mice. *Arrows* indicate epithelial cells. *Arrowheads* indicate nonepithelial cells. *Scale bar*: 20 μm. Significance was calculated using an unpaired *t* test. *P < .05, ***P < .001. CC3, cleaved caspase-3.
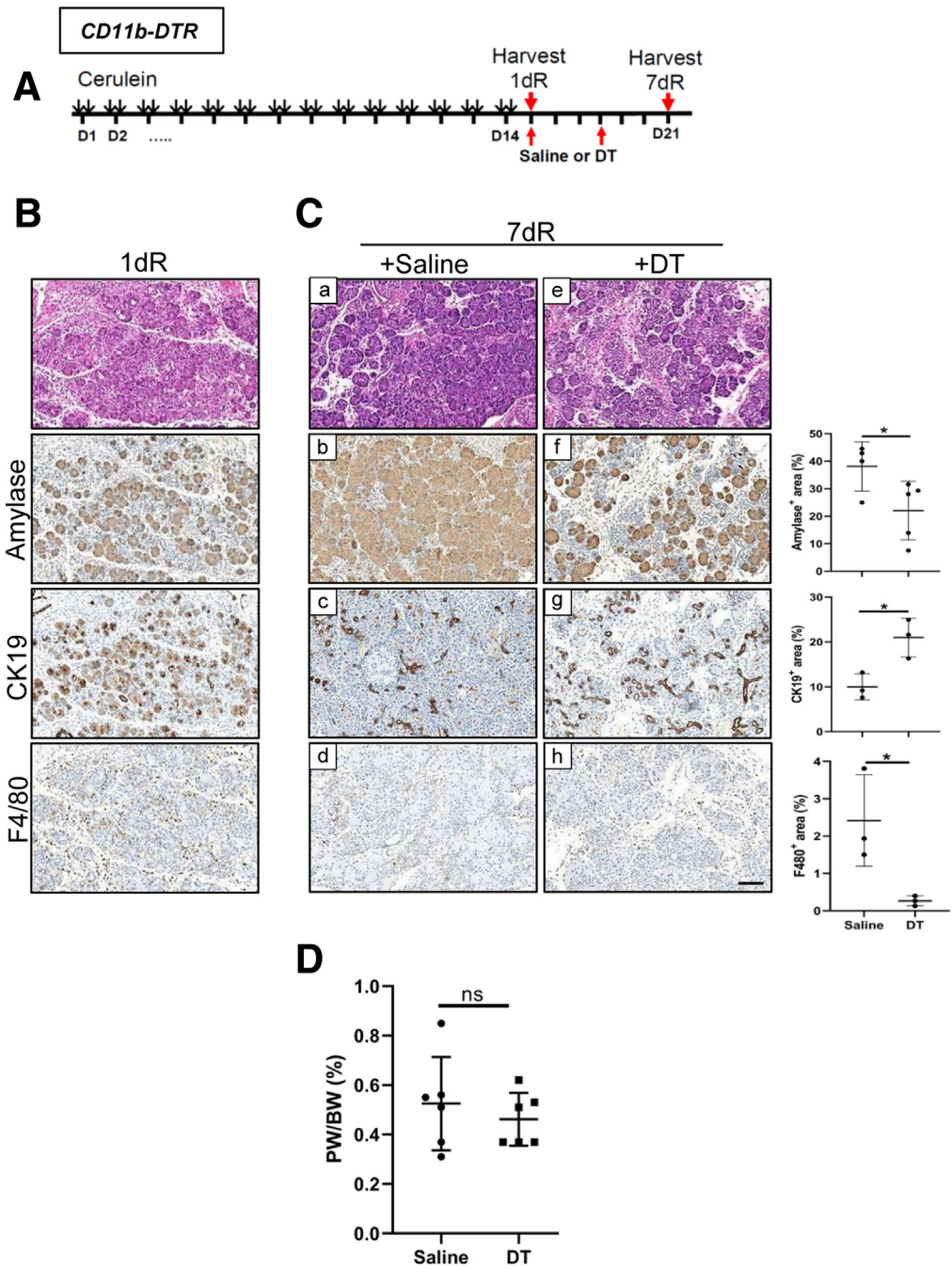
myeloid cells play an important role in the recovery of the pancreas from experimental pancreatitis.

HB-EGF Is Expressed in Macrophages During Pancreatitis

We and others have shown that EGFR/Mitogen-activated protein kinase kinase (MEK) signaling is critical for acinar cell proliferation and ADM.[9,11,29] In turn, macrophages are an abundant source of EGFR ligands in many disease states, including pancreatitis.[22,30] Given the decreased acinar cell proliferation upon myeloid cell depletion after pancreatic injury, we asked whether macrophage EGFR ligands may be responsible. First, we determined the expression of EGFR ligands in macrophages isolated from pancreata with 2-week cerulein treatment followed by 1- or 7-day recovery. To collect a sufficient number of macrophages for RNA analysis, CD45+;CD11b+;F4/80+ cells were sorted from a pool of pancreata (4–5 pancreata/cohort). Among 9 EGFR ligands examined, HB-EGF was expressed predominantly in macrophages from 1- and 7-day recovered tissue (Figure 2A). A panel of macrophage polarization marker genes suggested
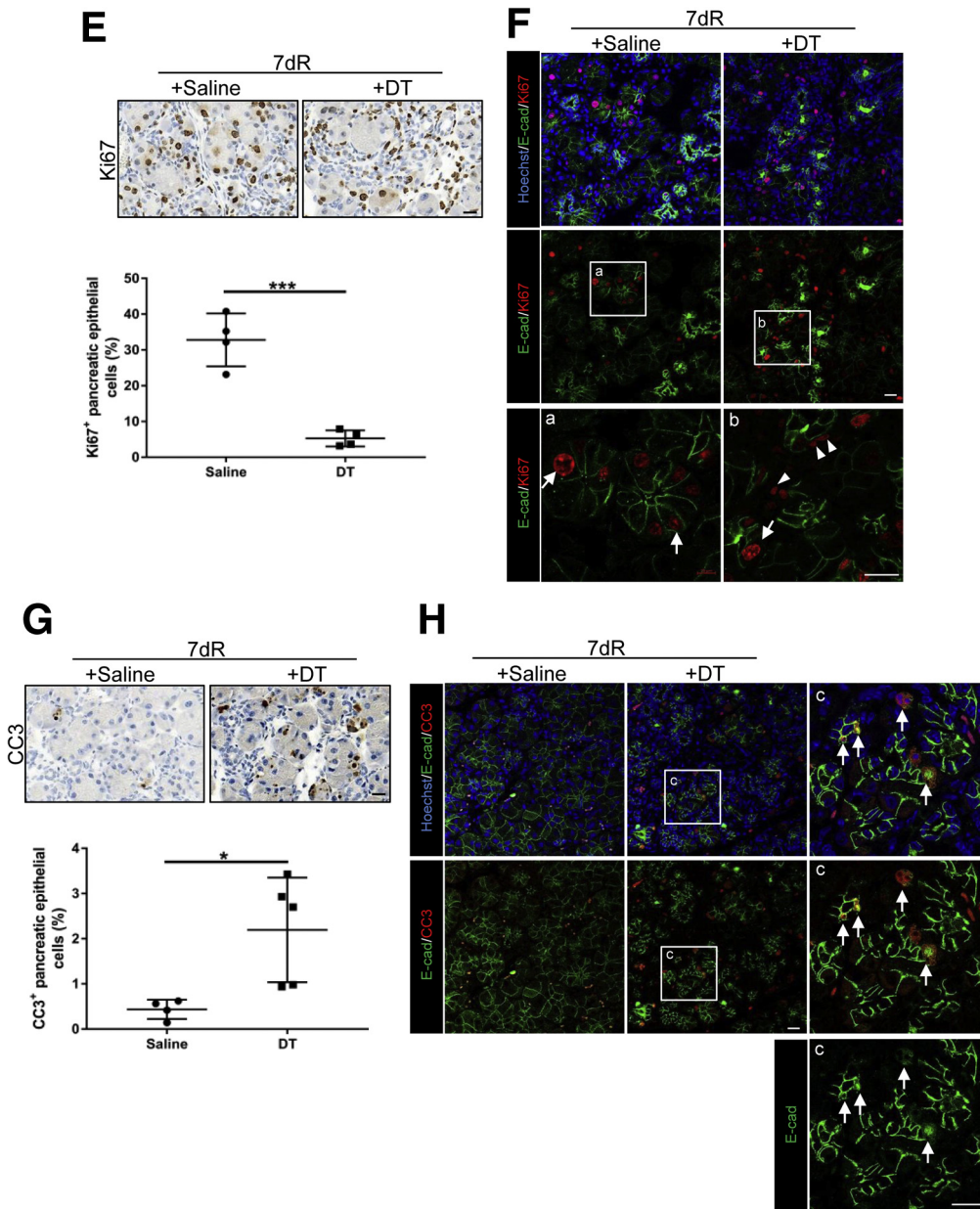
Figure 1. Continued

that the macrophages skewed toward alternatively activated macrophages in this model of experimental pancreatitis (Figure 2B), consistent with previous reports.[19]

Ablation of HB-EGF From Myeloid Cells Delays Pancreas Repair After Injury

To directly address whether HB-EGF derived from the myeloid cell compartment is involved in macrophage-dependent recovery after pancreatic injury, we generated *Hbegf^{f/f};LysM-Cre*[31,32] mice to ablate *Hbegf* specifically from myeloid cells. Eight-week-old *LysM-Cre* and *Hbegf^{f/f};LysM-Cre,* mice were treated with cerulein twice daily for 2 weeks followed by 1-, 3-, 5-, or 7-day recovery (Figure 3A). Both cohorts

of mice showed comparable initial damage at day 1 of recovery, with a similar relative pancreatic mass and histology, marked by acinar cell dropout, ADM, inflammatory cell infiltration, and abundant collagen deposition (Figure 3B, C, and E). However, unlike *LysM-Cre* control mice, whose relative pancreatic mass stabilized by 7 days after the last cerulein treatment, *Hbegf^{f/f};LysM-Cre* mice showed progressive pancreatic atrophy (Figure 3B and C). *LysM-Cre* pancreata showed few signs of injury after a 7-day recovery, marked by restoration of acinar tissue and resolution of the collagen-rich stroma. In contrast, *Hbegf^{f/f};LysM-Cre* pancreata had persistent ADM and unresolved fibrosis (Figure 3D).

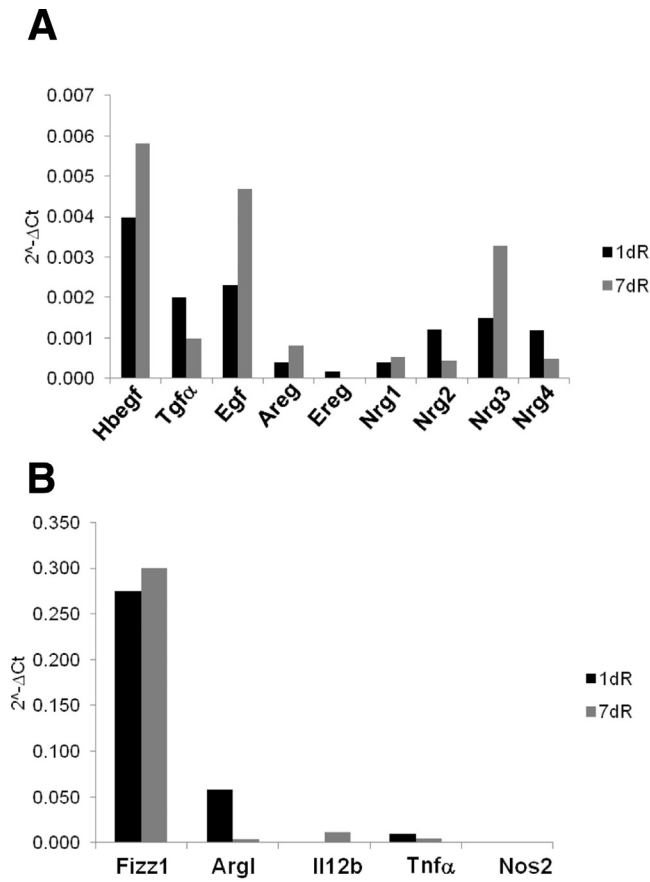Abundant macrophage infiltration was found in both *LysM-Cre* and *Hbegf^{f/f};LysM-Cre* pancreata at 1-day recovery,

A

B

Figure 2. Experimental pancreatitis is abundantly infiltrated with alternatively activated macrophages expressing EGFR ligands. Total RNA of macrophages (CD45+;CD11b+;F4/80+) was isolated from a pool of pancreata (4–5 pancreata/cohort) treated with cerulein after recovery for 1 or 7 days and analyzed by reverse-transcription quantitative PCR for (A) EGFR ligands and (B) macrophage markers. Alternatively activated macrophage markers are found in inflammatory zone protein (Fizz1) and arginase I (ArgI). Classically activated macrophage markers are Il12b, Tnfα, and nitric oxide synthase 2 (Nos2). Areg, amphiregulin; Egf, epidermal growth factor; Ereg, epiregulin; Tgf-α, transforming growth factor α; Nrg, neuregulin.

which decreased by 7 days, as determined by immunohistochemistry (IHC) (Figure 3E). By flow cytometry, there was no significant difference in the total number of CD45+ immune cells and CD45+;CD11b+ myeloid cells between the 2 cohorts, although there were slightly fewer CD45+;CD11b+;F4/80+ macrophages in *Hbegf*^f/f^;*LysM-Cre* pancreata compared with *LysM-Cre* controls at 1 day, but not 7 days, of recovery (Figure 3F). Consistent with previous results,[19] most infiltrating macrophages were CD45+;CD11b+;F4/80+;TNFα-;CD206+ (alternatively activated macrophages), with no significant difference detected in the 2 cohorts at either 1 or 7 days of recovery (Figure 3G). These results suggest that myeloid cell–derived HB-EGF does not affect the overall inflammatory response and is more likely acting directly within the local environment to restore pancreatic acinar cells after injury.

As in our earlier experiments, *LysM-Cre* pancreata had a substantial number of Ki67-positive parenchymal cells at both 1 and 7 days of recovery. In comparison, *Hbegf*^f/f^; *LysM-Cre* pancreata had approximately 3-fold fewer Ki67-positive cells (Figure 4A). The cyclin-dependent kinase inhibitor p21, which promotes cell-cycle arrest in G1, was detected in twice as many epithelial cells in *Hbegf*^f/f^;*LysM-Cre* pancreata compared with *LysM-Cre* control tissue (Figure 4B). Cell proliferation at 1 day of recovery also was assessed by bromodeoxyuridine (BrdU) incorporation. Similar to the Ki67 results, the number of BrdU+ cells in the *LysM-Cre* pancreata was significantly higher than that in *Hbegf*^f/f^;*LysM-Cre* pancreata (Figure 4C). IHC for cleaved caspase-3 showed 2-fold more apoptotic cells in *Hbegf*^f/f^;*LysM-Cre* pancreata compared with *LysM-Cre* controls at up to 5 days of recovery (Figure 4D); moreover, apoptotic cell death occurred primarily within the epithelium (E-cadherin positive) (Figure 4E) and not fibroblasts (α-smooth muscle actin positive) (Figure 4F). Collectively, these data suggest that the combination of decreased cell proliferation and increased apoptosis is responsible for continuing pancreatic atrophy in mice lacking myeloid cell–derived HB-EGF.

Myeloid-Derived HB-EGF Is Required for Resolution of DNA Damage During Recovery From Pancreatitis

DNA damage is common in inflammatory diseases, largely owing to an excess of reactive oxygen species (ROS) and reactive nitrogen species produced by inflammatory and epithelial cells.[33–35] On the other hand, macrophages facilitate DNA repair in a model of liver injury.[36] To test whether macrophages play a similar role in pancreatitis, we examined the formation of γH2AX nuclear foci. Histone H2AX phosphorylated at Ser139, referred to as γH2AX, flanks DNA double-strand breaks (DSBs) in response to DNA damage.[37] By IHC, γH2AX was significantly higher in the pancreata of DT-treated CD11b-DTR mice, compared with saline-treated controls (Figure 5A). Similarly, we observed very strong γH2AX foci in *Hbegf*^f/f^;*LysM-Cre* pancreata as early as day 1 of recovery compared with *LysM-Cre* controls, although the number of cells expressing γH2AX was similar. By 7 days of recovery, γH2AX positivity decreased sharply in *LysM-Cre* pancreata, but persisted in *Hbegf*^f/f^;*LysM-Cre* pancreata (Figure 5B). Because discrete γH2AX nuclear foci are a useful tool to highlight DSBs, we quantitated γH2AX nuclear punctate dots by immunofluorescence (Figure 5C, arrowheads). We found that *Hbegf*^f/f^;*LysM-Cre* pancreata had more DSBs than *LysM-Cre* pancreata (Figure 5D), and DNA damage occurred mainly in pancreatic epithelial cells (Figure 5E). We also noted that the staining pattern for γH2AX was not confined to nuclear punctate dots but also was observed as an annular staining of the outer portion of the nucleus (known as an apoptotic ring) and a pan-staining of the nucleus (Figure 5C and F, arrows).[38] These nonpunctate staining patterns are an indicator of DNA damage-induced apoptotic cell death.[38] Indeed, cleaved caspase-3 co-stained cells with γH2AX apoptotic
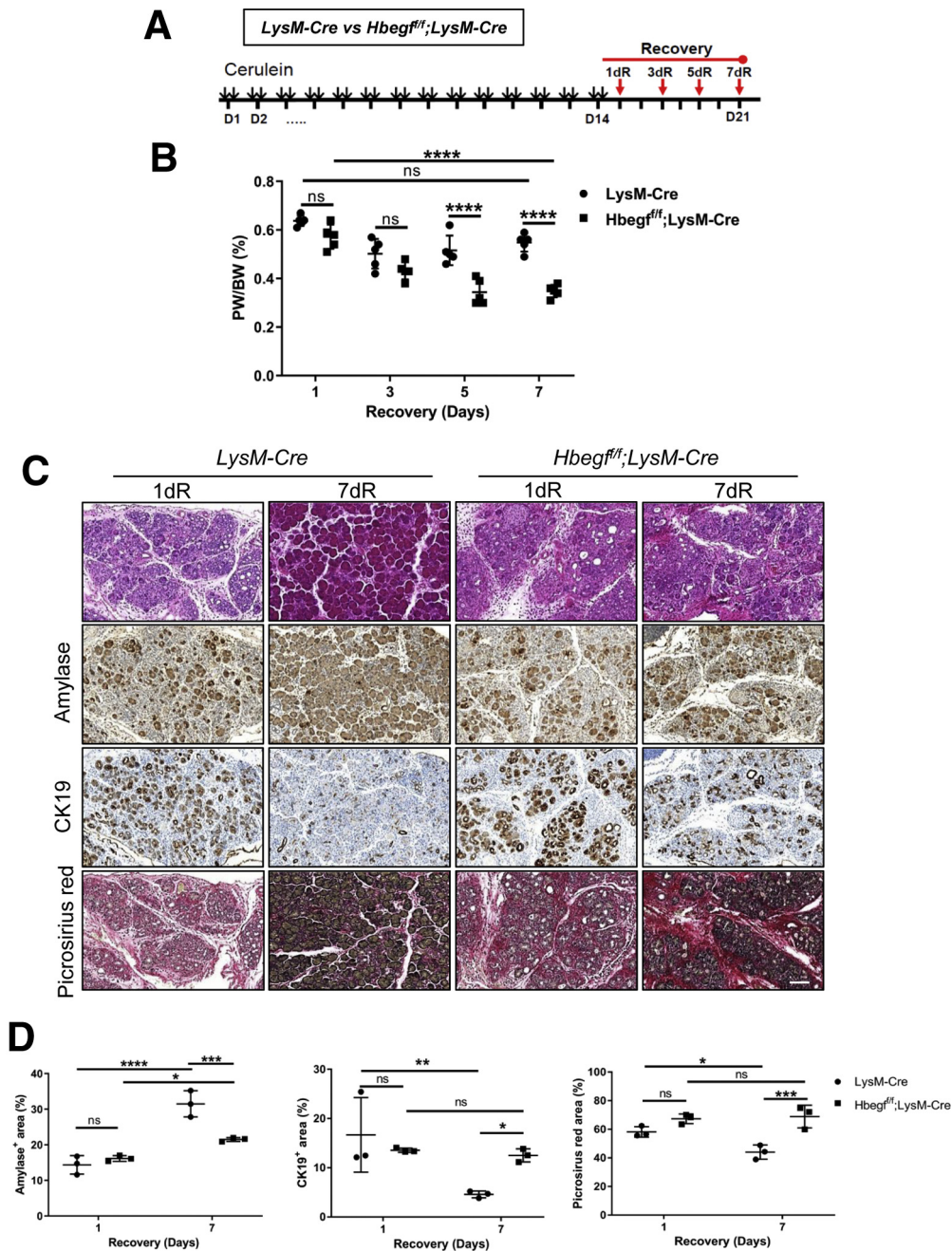
Figure 3. Ablation of HB-EGF from myeloid cells results in continuing pancreatic atrophy during recovery. (*A*) Schematic of cerulein treatment protocol for *LysM-Cre* and *Hbegf^{f/f};LysM-Cre* mice. (*B*) Analysis of pancreas-to-body weight ratios (PW/BW) of mice with 2-week cerulein treatment and recovery for 1, 3, 5, and 7 days (n = 5). Significance was calculated by 2-way analysis of variance with the Tukey multiple comparison. (*C* and *E*) Pancreas sections were analyzed by H&E staining and IHC for amylase, CK19, picrosirius red, and F4/80. *Scale bars*: (C) 100 μm, (E) 200 μm. (*D* and *E*) Quantitation of amylase-positive area, CK19-positive area, picrosirius red–positive area, and F4/80 positive area (n = 3). Significance was calculated using 2-way analysis of variance with Fisher's LSD (least significant difference). (*F* and *G*) Pancreas sections were analyzed for immune cells by flow cytometry. (*F*) Percentage of immune cells (CD45$^+$), myeloid cells (CD45$^+$;CD11b$^+$), and macrophages (CD45$^+$;CD11b$^+$;F4/80$^+$) is indicated. (*G*) Macrophages (CD45$^+$;CD11b$^+$;F4/80$^+$) were analyzed further for different subtypes by labeling with TNF-α and CD206 antibodies (n $\geq$ 3). Significance was calculated by 2-way analysis of variance with Tukey multiple comparison. *$P <$ .05, **$P <$ .01, ***$P <$ .001, and ****$P <$ .0001.

rings and pan-nuclear staining (Figure 5*F*, arrows), but not cells with γH2AX nuclear punctate dots (Figure 5*F*, arrowheads). Consistent with the overall increase in cell death in mutant mice, we found a greater number of γH2AX apoptotic patterns in pancreata from *Hbegf^{f/f}; LysM-Cre*, compared with control (Figure 5*G*). These data suggested that ablation of myeloid cell HB-EGF impairs the DNA repair response, leading ultimately to cell death.
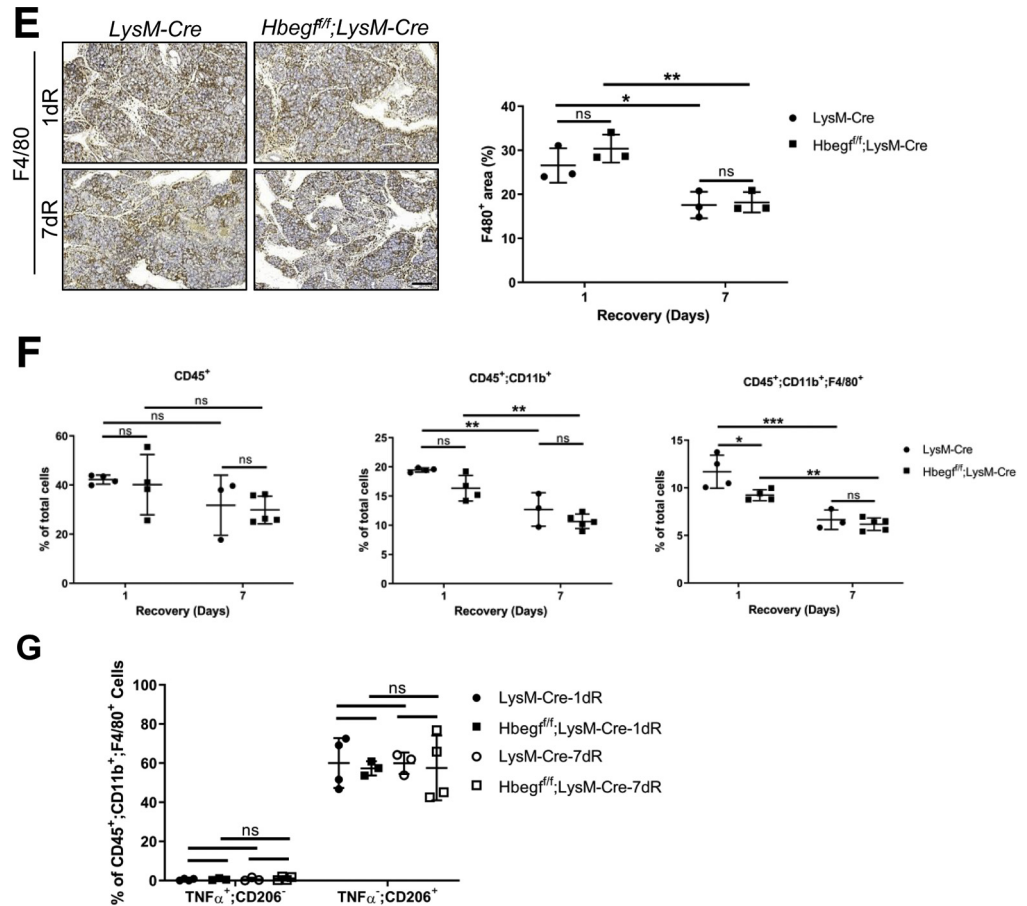
E

F

G

Figure 3. Continued

Soluble HB-EGF Promotes Resolution of DNA Damage in Pancreatic Cells In Vitro

The unresolved accumulation of γH2AX in *Hbegf^f/f;LysM-Cre* pancreata long after cessation of cerulein treatment led us to investigate the role of HB-EGF in DNA repair in pancreatic acinar cells. To dissect this mechanism, we used the mouse pancreatic acinar cell line 266.6 to study the role of soluble HB-EGF (sHB-EGF) in DNA repair in response to H_2O_2-induced DNA damage. The cells were treated with H_2O_2 for 1 hour to induce DNA damage followed by HB-EGF incubation for the indicated times. We found that γH2AX accumulation was induced within 1 hour of H_2O_2 treatment and continued to accumulate for 2 hours after washing away H_2O_2; in comparison, addition of sHB-EGF caused a rapid decrease in γH2AX within 1 hour after treatment (Figure 6A).

Histone H4 methylated at lysine residue 20 (H4K20) plays diverse roles in cellular processes based on the degree of methylation. Monomethylation of H4K20 (H4K20me1) is associated mainly with cell-cycle progression, whereas H4K20me2 becomes a mediator for DNA damage checkpoint activation.[39] Monomethylation and dimethylation of H4K20 is regulated by nuclear EGFR in response to EGF and ionic radiation.[40] Similar to EGF, HB-EGF is capable of inducing EGFR translocation to the nucleus.[41] To test if this

mechanism is in play in pancreatitis, we found that addition of sHB-EGF after inducing DNA damage efficiently increased the level of H4K20me1 within 1 hour. Subsequently, the level of H4K20me2 was increased within 2 hours as it was converted from H4K20me1 (Figure 6A). To directly measure DNA breaks, we performed a "comet assay." In this assay, DNA breaks are visualized using electrophoresis, with damaged DNA (the tail) trailing the intact DNA (the head) resembling a comet.[42] One-hour H_2O_2 treatment strongly induced DNA strand breaks in the 266.6 cells, as determined by measuring the length of the comet tail. Because sHB-EGF was supplemented after H_2O_2 removal, DNA in the comet tails was rapidly shifted to the comet heads within 3 hours, indicating that sHB-EGF promoted DNA repair (Figure 6B).

To test for EGFR nuclear translocation, 266.6 cells were treated with H_2O_2 followed by sHB-EGF. Cytoplasmic and nuclear fractions were collected and immunoblotted for EGFR. Nuclear EGFR levels were increased significantly within 15 minutes of sHB-EGF treatment after H_2O_2 stimulation, decreasing to a level similar to that in cells treated with HB-EGF alone within 45 minutes. EGFR remained in the cytoplasmic fraction in cells not treated with sHB-EGF after H_2O_2 removal (Figure 6C). Total EGFR levels were decreased in cells treated with sHB-EGF after 30 minutes of stimulation (Figure 6C), consistent with proteasome-mediated
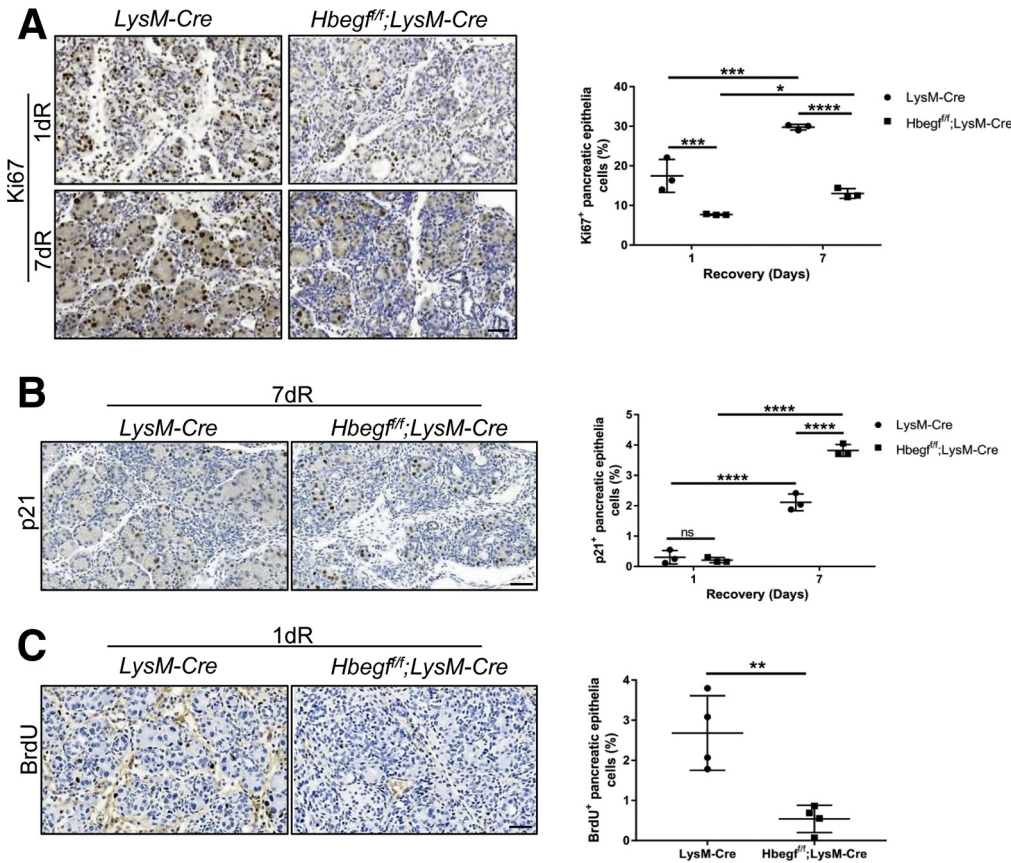
Figure 4. Myeloid HB-EGF is required for parenchymal cell survival. (A–D) IHC (left) for Ki67, p21, BrdU, and CC3 on pancreas sections from LysM-Cre and Hbegf[f/f];LysM-Cre mice with 1 or 7 days of recovery after 2-week cerulein treatment. Scale bars: 50 μm. Quantitation (right) of Ki67, p21, BrdU, and cleaved caspase 3 (CC3)-positive pancreatic epithelial cells (n ≥ 3). Significance was calculated (C) using an unpaired t test and (A, B, D) 2-way analysis of variance with Fisher's least significant difference (LSD). (E and F) Representative immunofluorescent images for (E) CC3 (green), Hoechst33342 (blue), and E-cadherin (E-cad) (red) or (F) α-smooth muscle actin (α-SMA) (red) on 1-day recovery pancreata of LysM-Cre and Hbegf[f/f];LysM-Cre mice. Scale bar: 20 μm. *P < .05; **P < .01; ***P < .001; and ****P < .0001.

turnover after receptor activation.[43] To further show that sHB-EGF–stimulated DNA repair is EGFR dependent, small interfering RNA (siRNA)-mediated knockdown of EGFR was performed. Knockdown of EGFR in 266.6 cells resulted in a concomitant decrease in dimethylated H4K20 formation and persistent accumulation of γH2AX, both indicative of inefficient DNA repair (Figure 6D). These findings suggest that upon DNA damage, sHB-EGF enhances EGFR nuclear translocation, which, in turn, regulates H4K20 methylation and subsequent DNA repair.

Myeloid Cell–Derived HB-EGF Regulates DNA Repair In Vivo

To test if our in vitro findings accurately reflect the in vivo condition, we first stained experimental pancreatitis tissue for EGFR to examine nuclear translocation. Unfortunately, under these conditions, nuclear EGFR was beneath the level of detection by IHC or immunofluorescence. We turned instead to the downstream consequences of EGFR translocation, such as H4K20 methylation, to test for myeloid cell HB-EGF–dependent regulation. IHC for H4K20me2 in day 1 recovered pancreata showed that LysM-Cre pancreata had more H4K20me2+ epithelial cells than Hbegf[f/f];LysM-Cre pancreata (Figure 7A, arrows). Co-immunofluorescence

staining for H4K20me2, E-cadherin, and α-smooth muscle actin showed that H4k20me2 formed nuclear punctate dots mainly in epithelial cells (E-cadherin+) (Figure 7B, arrows). Because H4K20me2 is responsible for recruitment of the DNA repair factor p53-binding protein 1 to sites of DNA damage,[44] we quantitated cells containing p53-binding protein 1 nuclear foci after 1 day of recovery. Consistent with our H4K20me2 results, Hbegf[f/f];LysM-Cre pancreata had fewer 53BP1+ cells (Figure 7C). Together, these results indicated that myeloid cell–derived HB-EGF regulates the cascade of H4K20 methylation and 53BP1 recruitment to damaged chromatin, promoting efficient DNA repair after pancreatic damage.

EGFR Is Required for Efficient DNA Repair During Recovery From Pancreatitis

Our inability to detect nuclear EGFR in vivo prompted us to test if EGFR is, in fact, critical for resolving DNA damage after pancreatic wounding as our data would suggest. Unfortunately, pancreas-specific ablation of EGFR before cerulein treatment completely protects the pancreas from cerulein-induced ADM and formation of the fibroinflammatory stroma.[9] The lack of inflammatory microenvironment resulting in no obvious DNA damage makes this model inappropriate for testing the role of EGFR specifically during the recovery phase. Likewise, efficient ablation
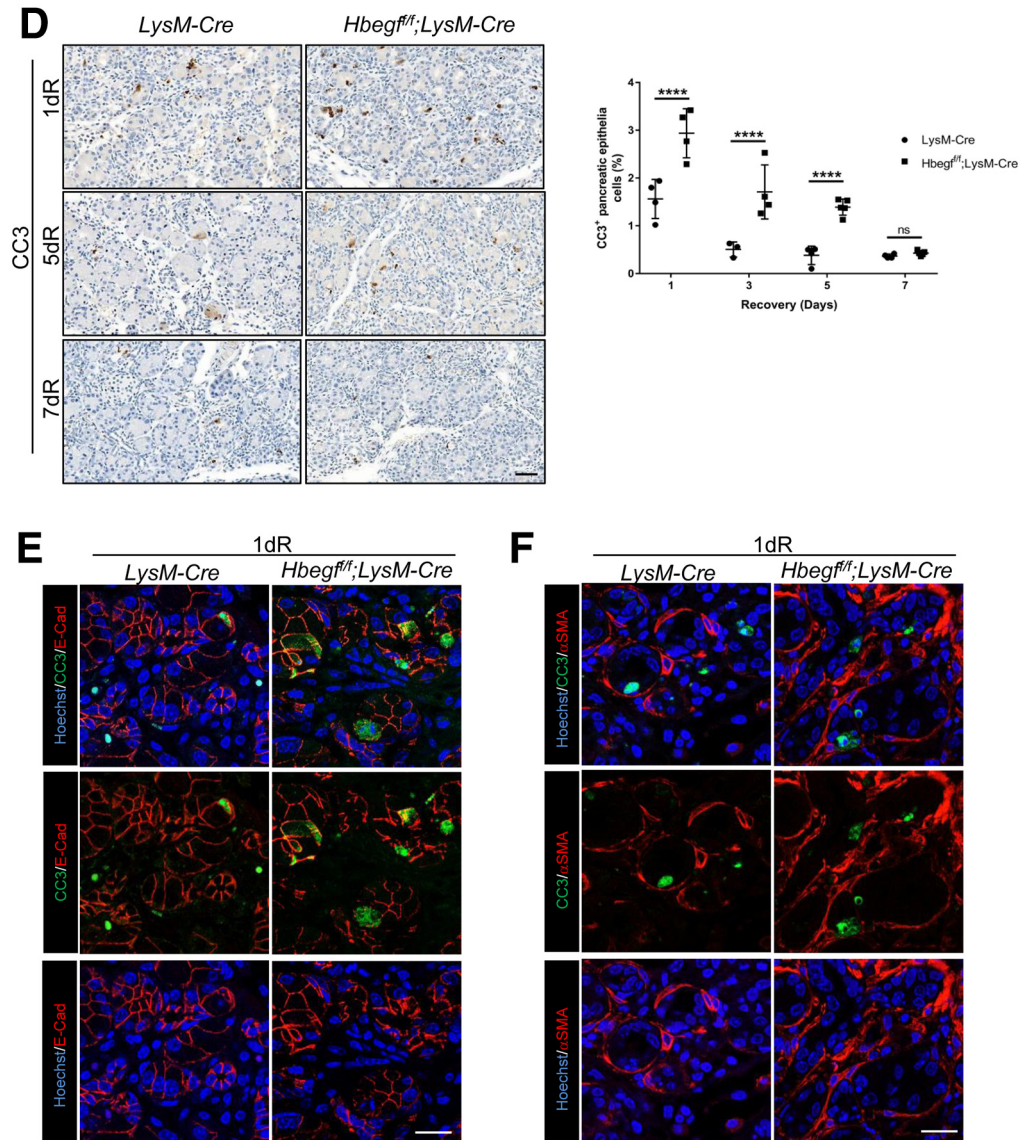
Figure 4. Continued

specifically after wounding using tamoxifen-induible Cre recombinase (Cre^ERT) models was impossible because in existing Cre^ERT models, expression is dependent on the differentiation status of target cells (ie, acinar vs metaplastic duct cells). To overcome these limitations, we developed the $Egfr^{f/f};Ptf1a^{FlpO/+};FSF\text{-}Rosa26^{CAG\text{-}CreERT2}$ mouse. The novel $Ptf1a^{FlpO/+}$ allele has a codon-optimized Flp recombinase (FlpO) knocked into the $Ptf1a$ locus, driving FlpO expression and flippase recognition target (Frt)-based recombination (Figure 8A). Surprisingly, unlike the $Ptf1a^{Cre}$ driver line, which efficiently directs loxP-mediated recombination in pancreas progenitor cells, resulting in recombination in most adult parenchymal cells,[45] lineage tracing showed that $Ptf1a^{FlpO}$–driven FRT-mediated recombination largely bypassed islet and duct cell recombination, suggesting inefficient recombination in the pancreatic progenitors, with efficient recombination primarily limited to adult acinar cells (Figure 8B). By crossing $Ptf1a^{FlpO}$ mice to mice carrying

a tamoxifen-inducible Cre^ERT transgene under the control of a universal CMV enhancer, chicken beta-actin promoter (CAG), interrupted by an Frt-flanked transcriptional/translational stop (STOP) cassette (FSF) and knocked into the ROSA26 locus ($FSF\text{-}Rosa26^{CAG\text{-}CreERT2}$),[46] we created a model that allows us to induce Cre-lox recombination in acinar-derived cells independent of their plastic differentiation status in pancreatitis (Figure 9A).

To study tissue recovery after experimental pancreatitis, $Egfr^{f/f};Ptf1a^{FlpO/+};FSF\text{-}Rosa26^{CAG\text{-}CreERT2}$ mice were treated for 2 weeks with cerulein followed by 7 days of recovery. To knockout EGFR in pancreatic epithelial cells specifically during the recovery phase, tamoxifen was administered on day 13 of cerulein treatment for 3 consecutive days (Figure 9A). Control mice from an identical genotype were treated with vehicle in place of tamoxifen. Because the majority of acinar cells in the vehicle-treated mice were redifferentiated from metaplastic ducts after 7 days of recovery, the EGFR level was
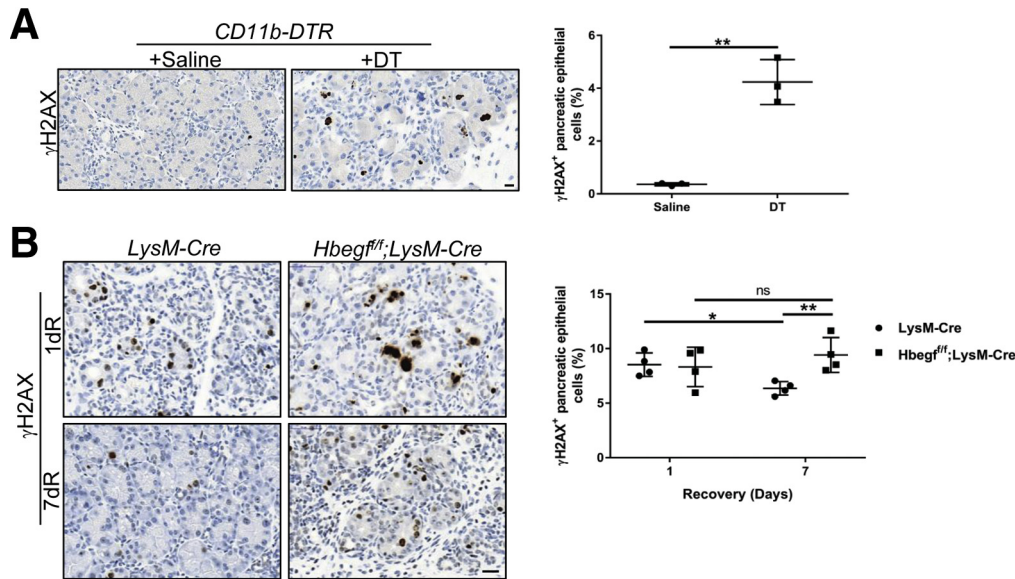
Figure 5. Ablation of myeloid HB-EGF slows DNA damage repair in parenchymal cells. (*A* and *B*) IHC for γH2AX on pancreas sections from (*A*) *CD11b-DTR* mice with 7-day recovery and (B) *LysM-Cre* and *Hbegf^f/f^;LysM-Cre* mice with 1 and 7 days of recovery. *Scale bar*: 20 μm. Quantitation of γH2AX-positive pancreatic epithelial cells (n ≥ 3). (*C*) Representative immunofluorescent images for γH2AX (green), CD45 (red), and Hoechst33342 (blue) on pancreas sections of *Hbegf^f/f^;LysM-Cre* mice with 2-week cerulein and 1-day recovery. *Scale bar*: 20 μm. (*D*) Quantitation of γH2AX nuclear foci (n = 3). CD45^+ immune cells (red) were excluded from quantitation. (*E* and *F*) Representative immunofluorescent images for Hoechst33342 (blue), γH2AX (green), α-smooth muscle actin (SMA) (white), and (*E*) E-cad or (*F*) cleaved caspase 3 (CC3) (red) on 1-day recovery pancreata of *LysM-Cre* and *Hbegf^f/f^;LysM-Cre* mice. *Arrowheads* indicate γH2AX nuclear punctate *dots*. *Arrows* indicate γH2AX apoptotic patterns. *Scale bars*: (E) 20 μm, (F) 10 μm. (*G*) Quantitation of γH2AX apoptotic patterns includes cells containing γH2AX-ring staining, nuclear pan staining, and staining on apoptotic bodies (n = 3). Significance was calculated using 2-way analysis of variance with Tukey multiple comparison. *$P < .05$, **$P < .01$, and ****$P < .0001$.

rarely detectable. Thus, pancreata were harvested at 24 hours after tamoxifen/vehicle for detecting EGFR expression. Pancreata from tamoxifen-treated mice showed widespread loss of EGFR on epithelial membranes compared with vehicle control (Figure 9B). Upon initial observation at 7 days of recovery, there were no apparent differences between cohorts, reflecting the complex role of EGFR in maintaining ADM.[9] Relative pancreas mass and cell proliferation of the EGFR knockout and control pancreata were not different and histologic examination of the pancreata showed a similar level of acinar cell recovery by 7 days after cerulein treatment (Figure 9C). These results are consistent with our previous finding that MEK activation is required to sustain ADM.[11] However, similar to the *Hbegf^f/f^;LysM-Cre* phenotype, we found that the number of cells with γH2AX accumulation persisted in EGFR knockout pancreata (Figure 9C), indicating that ablation of EGFR in pancreatic epithelial cells indeed impair DNA repair. Moreover, unrepaired DNA ultimately resulted in cell death, showed by a concomitant increase in cleaved caspase 3 in EGFR ablated pancreata (Figure 9C). These results support an essential function for a paracrine HB-EGF/EGFR loop in DNA repair after pancreatic wounding.

Discussion

In response to tissue injury, pancreatic acinar cells transdifferentiate to proliferative metaplastic ducts that are capable of partially regenerating acinar cell mass.[10,47,48] Our previous studies showed that the EGFR-MEK signaling axis is required for acinar cell proliferation and ADM, in part through acinar cell autonomous signaling.[9,11] However, the role of macrophages in these early processes has been implicated,[18,49] suggesting a critical role for paracrine signaling. Macrophages express abundant EGFR ligands, with HB-EGF expression a prominent feature of macrophages that infiltrate the wound site.[22] Here, we found that myeloid-derived HB-EGF has no effect on initiation of EGFR-dependent ADM formation during cerulein-induced pancreatitis, consistent with this process being initiated by parenchymally derived ligands.[9] On the other hand, myeloid-derived HB-EGF plays a unique and profound role in promoting epithelial DNA repair, a function for which other EGFR ligands emanating from the damaged epithelium or stroma are clearly insufficient.

The delayed recovery from experimental pancreatitis when either myeloid cells were depleted or myeloid HB-EGF was ablated was evident from the failure to restore the acinar cell population. However, pancreatic tissue atrophy was observed only in the *Hbegf^f/f^;LysM-Cre* mice, a difference possibly attributable to the absence of myeloid HB-EGF throughout the entirety of pancreatitis initiation and tissue recovery, whereas myeloid cell depletion was initiated beginning 1 day after cerulein treatment.
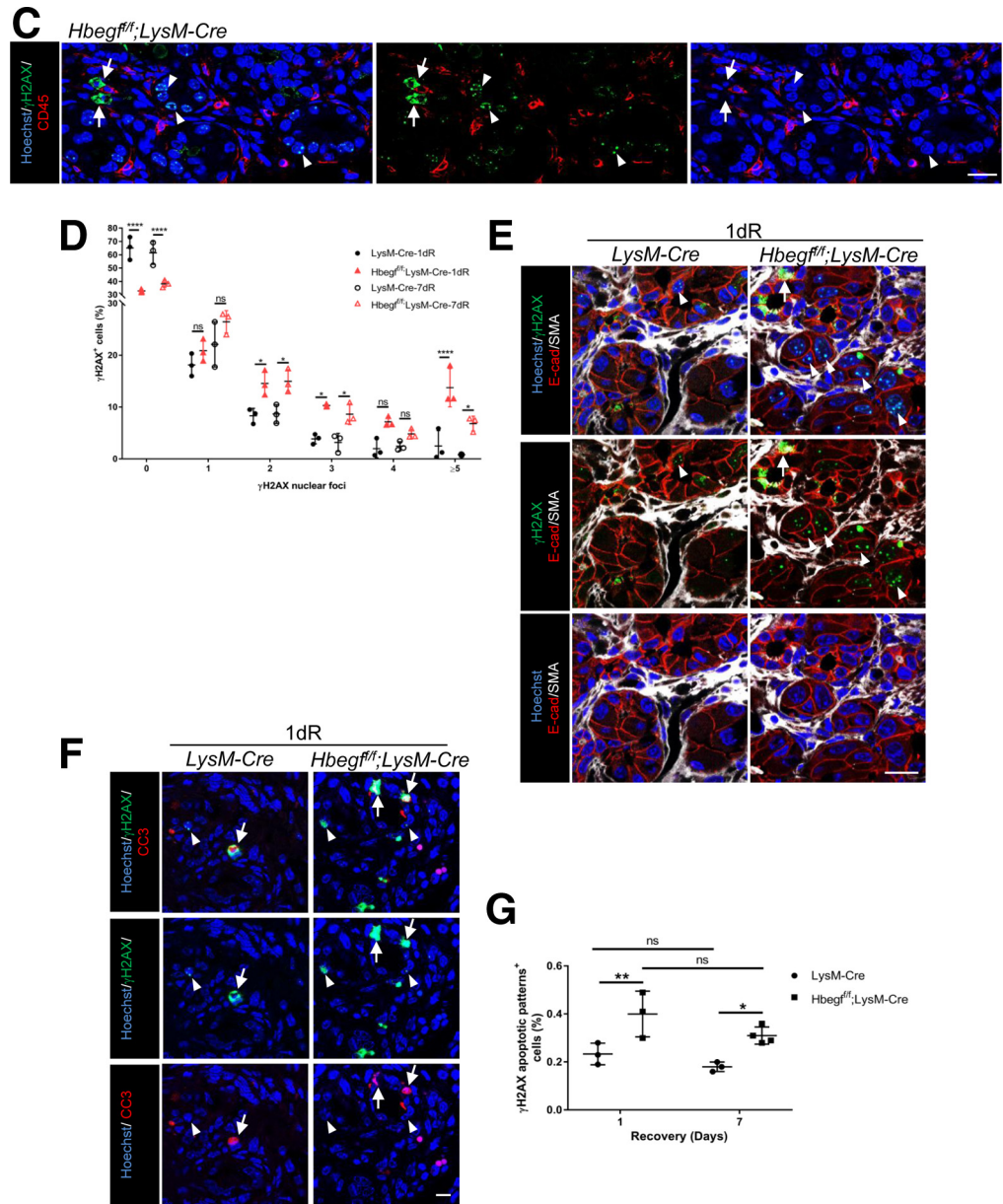
Figure 5. Continued

Epithelial cell proliferation was significantly lower in mice lacking myeloid HB-EGF, as determined by Ki67 expression and BrdU incorporation. Together with high levels of p21 expression, this indicates that without myeloid HB-EGF, pancreatic epithelial cells arrest in the G1 phase of the cell cycle, consistent with a defective DNA damage response.[50] Cell-cycle arrest induced by DNA damage checkpoints allow time for repair before initiating DNA synthesis. Unrepaired DNA lesions ultimately enforce permanent growth arrest or cell death.[50] We found that $\gamma H2AX^+$ DSBs persisted in mice lacking myeloid HB-EGF through 7 days of recovery. This persistent DNA damage was associated with an increased level of DNA damage-associated cell death, identified by both $\gamma H2AX^+$ apoptotic

patterns and cleaved caspase-3. This enhanced level of apoptotic cell death, together with the muted proliferative response, likely contributes to the dramatic progressive pancreatic atrophy long after the cessation of tissue damage.

In response to DNA damage, $\gamma H2AX$ serves as a platform on DNA breaks for the initial recruitment and retention of DNA repair factors, such as 53BP1. In mice lacking myeloid HB-EGF, we find less focal enrichment of 53BP1 in pancreatic epithelia even as $\gamma H2AX$ continues to accumulate. Recruitment of 53BP1 to damaged chromatin is associated with various histone modifications, including histone H4 methylation at lysine 20.[44] H4K20me2 has been linked to DNA damage response because it physically

interacts with and stabilizes 53BP1.[51,52] Consistent with the defect in 53BP1 recruitment, we found a decrease in H4K20me2 in pancreatic epithelia in *Hbegf^{f/f};LysM-Cre*

pancreata. In vitro, addition of ectopic HB-EGF increases the level of H4K20me2, which correlates to a decrease in γH2AX levels.
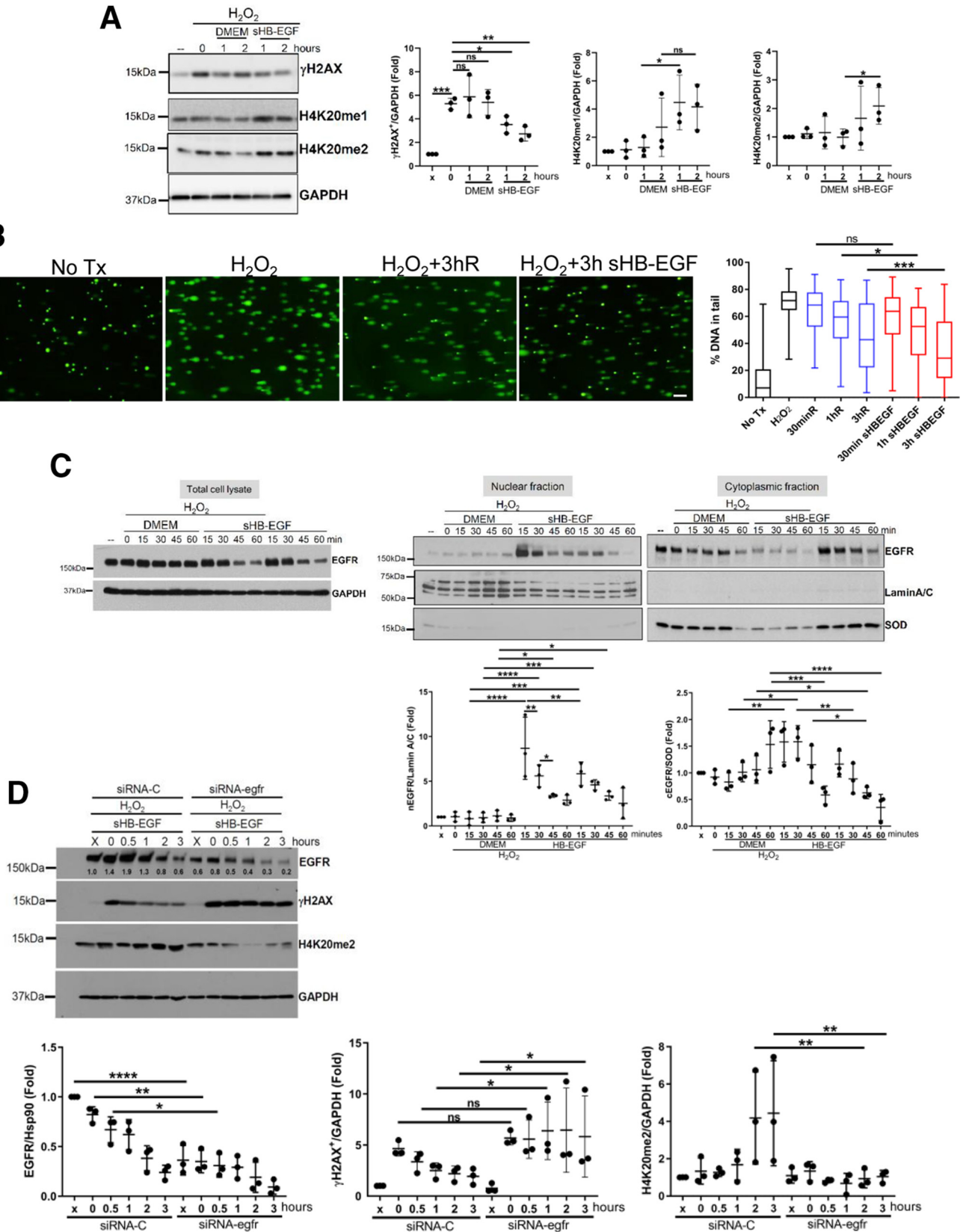
Figure 7. Myeloid HB-EGF activates the DNA repair process in pancreatitis in vivo. (*A* and *B*) IHC for H4K20me2 and representative immunofluorescent images for Hoechst33342 (blue), α-smooth muscle actin (SMA) (white), E-cadherin (E-cad) (red), and H4K20me2 (green) on 1-day recovery pancreatic sections of *LysM-Cre* and *Hbegf^f/f^;LysM-Cre* mice. *Arrowheads* and *arrows* show H4K20me2-positive staining in stromal and epithelial cells, respectively. *Scale bars*: 20 μm. Quantitation of H4K20me2-positive epithelial cells (n = 3). (*C*) Representative immunofluorescent images for Hoechst33342 (blue), CD45 (red), and 53BP1 (green) on 1-day recovery pancreatic section of *LysM-Cre* and *Hbegf^f/f^;LysM-Cre* mice. *White arrows* show nuclear foci of 53BP1. *Scale bar*: 10 μm. Quantitation of 53BP1-positive cells. CD45⁺ cells were excluded from quantitation. Significance was calculated using an unpaired *t* test. *P < .05.
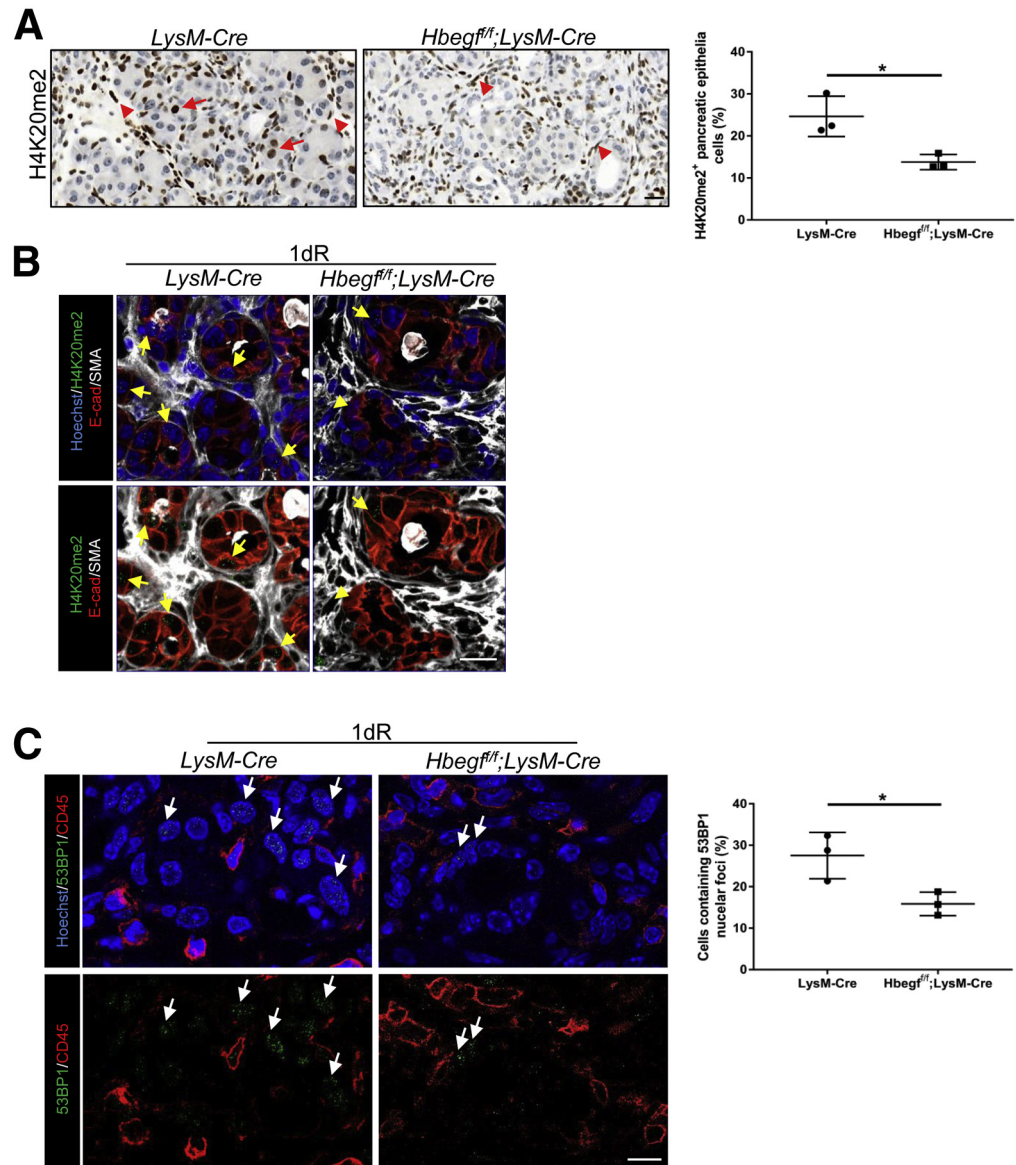
Nuclear EGFR has been suggested to be a regulator of H4K20 methylation in response to ionizing radiation and EGF.[40] We found that HB-EGF is capable of inducing EGFR nuclear translocation, an effect that is further enhanced when cells have DNA damage. Nuclear EGFR was difficult to detect in vivo, presumably because it turns over rapidly in response to HB-EGF, consistent with our in vitro experiments. We previously showed that ablating parenchymal

Figure 6. (*See previous page*). Soluble HB-EGF promotes DNA repair through EGFR in vitro. (*A* and *C*) The 266.6 cells were exposed to 500 μmol/L H_2O_2 for 1 hour followed by treatment with/without sHB-EGF for the indicated times. (*A*) Whole-cell lysates were analyzed by immunoblotting for γH2AX, H4K20me1, H4K20me2, and glyceraldehyde-3-phosphate dehydrogenase (GAPDH) (a loading control). (*C*) Cytosolic and nuclear fractions were isolated from 266.6 cell lysates. EGFR was analyzed by immunoblotting. Lamin A/C and β-tubulin were used as loading and purity controls for nuclear and cytosolic fractions, respectively. (*B*) Representative images of comet assay from 266.6 cells treated with nothing (no Tx) or H_2O_2 in serum-free DMEM for 1 hour followed by 3-hour recovery in DMEM (H_2O_2+3hR) or sHB-EGF supplement (H_2O_2+3h sHB-EGF). Quantitation of DNA in the comet tail was performed by analyzing 150 cells for each sample from 3 separate independent experiments. *Scale bar*: 200 μm. (*D*) EGFR knockdown was performed in 266.6 cells transfected with siRNA control (siRNA-C) or siRNA against EGFR (siRNA-egfr). At 48 hours after transfection, cells were treated with H_2O_2 for 1 hour followed by HB-EGF treatment for the indicated time. Cell lysates were analyzed by immunoblotting for EGFR, γH2AX, H4K20me2, and GAPDH. Significance was calculated by 1-way analysis of variance with (*A, C, D*) Fisher's LSD and (*B*) with Tukey multiple comparison test. *P < .05, **P < .01, ***P < .001, and ****P < .0001.
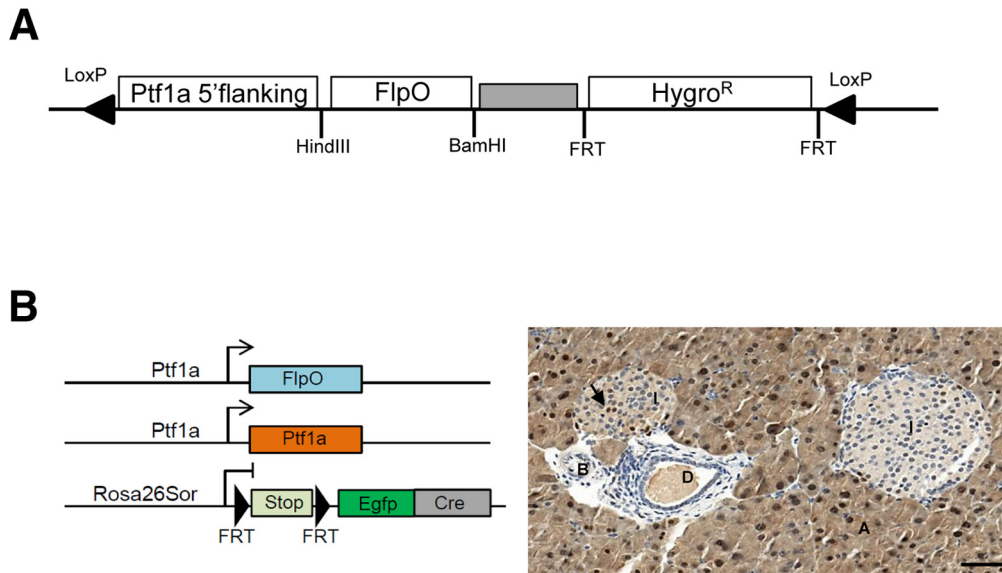
A

B

Figure 8. FlpO-mediated recombination on pancreas. (*A*) Design of the *Ptf1a*$^{FlpO(HygroR)}$ cassette exchange vector. The FlpO open reading frame was inserted into an exchange vector containing 2 inverted LoxP sites and used to perform recombinase-mediated cassette exchange in embryonic stem cells containing a loxed cassette acceptor allele in the *Ptf1a* gene locus that also had 2 inverted LoxP sites. A hygromycin resistance gene (Hygro^R), flanked by tandem FRT sites, was inserted at the 3'-end of the exchange vector for positive selection during recombinase-mediated cassette exchange. *Gray box*, rabbit β-globin intron 2 plus 3'-untranslated region. (*B*) IHC for green fluorescent protein (GFP) visualized the expression of EGFP-Cre fusion protein in the pancreas of a 6-week-old *Ptf1a*$^{FlpO/+}$;*R26*^{MASTR} reporter mouse. The *arrow* shows a GFP-positive cell in the islet. *Scale bar*: 50 μm. A, acini; B, blood vessel; D, pancreatic duct; I, islet.

EGFR before cerulein treatment protects the pancreas from cerulein-induced ADM and formation of the fibroinflammatory stroma,[9] initially preventing us from testing if EGFR does play a role in vivo during recovery from injury. To bypass this limitation, we created a novel conditional EGFR knockout mouse (*Egfr*$^{f/f}$;*Ptf1a*$^{FlpO/+}$;*Rosa*$^{CreER/+}$) that allows us to leave EGFR intact during the damage phase of experimental pancreatitis but to ablate it specifically in pancreatic epithelia cells only during recovery. Surprisingly, we did not detect tissue atrophy or a delay of acinar cell recovery with EGFR ablation, possibly owing to EGFR's role in maintaining ADM, a function suggested by our previous studies.[9,11] Nonetheless, we did find significant accumulated DNA damage in the pancreata with a lack of EGFR, consistent with the specific role of HB-EGF in this aspect of tissue healing.

DNA damage is the most significant consequence of oxidative stress.[53] Tobacco smoke and alcohol consumption, the most common stimuli of pancreatitis in people, can dramatically increase ROS, resulting in oxidative stress.[34,35] Subsequently, abundant inflammatory cell infiltration into the injured pancreas leads to a microenvironment rich in ROS. In parallel, cerulein, used here to induce tissue damage, stimulates nicotinamide adenine dinucleotide phosphate oxidase (NADPH oxidase) activity in acinar cells to produce ROS, leading to the recruitment of inflammatory cells.[54] Inflammation has the potential to increase ROS further, increasing DNA damage, which can lead to cell death if not resolved.[33]

Consistent with their contribution to tissue damage, others have shown that macrophage ablation before the induction of experimental pancreatitis is protective.[18] Here, we find that macrophage ablation specifically during the healing phase of experimental pancreatitis stymies tissue repair and prevents the resolution of DNA damage. Macrophage-enhanced DNA repair was seen previously in the livers of mice treated with diethylnitrosamine. This response reportedly was blocked by systemic administration of CRM197,[36] an HB-EGF inhibitor that specifically recognizes the human form of HB-EGF, but does not recognize the mouse protein.[55] To avoid this controversy, we generated conditional knockout mice targeting myeloid HB-EGF and parenchymal EGFR. With these unique and precise models we have definitively identified that macrophages promote pancreatic wound healing by producing HB-EGF to stimulate epithelial EGFR-mediated DNA repair, suggesting that HB-EGF could be used in therapy for pancreatitis. However, if the inflamed microenvironment also leads to oncogenic mutation in *KRAS* in the epithelium, stimulation of EGFR/MEK signaling also will promote tumorigenesis.[9,29,56] Our results emphasize that targeting the complex activities of pancreas disease-associated macrophages demands cautious scrutiny.

Methods
Mice

All animal experiments and procedures were conducted with the approval of the Institutional Committee on Use and Care of Animals at the University of Michigan.

Figure 9. Ablation of EGFR during recovery from pancreatitis delays resolution of DNA damage. (*A*) Genetic strategy and schematic of cerulein treatment protocol to ablate *Egfr* from the parenchyma by tamoxifen-mediated activation of Cre[ERT2]. Pancreata were harvested after 7 days of recovery after cerulein (*red arrow*). (*B*) H&E staining and IHC for EGFR on pancreata of *Egfr[f/f];Ptf1a[FlpO/+]; R26[CreERT/+]* mice were harvested 1 day after vehicle/tamoxifen treatment after 2 weeks of cerulein. The boxes are the magnified area. *Scale bar*: 20 μm. (*C*) Pancreas sections were analyzed by H&E staining and IHC for Ki67, BrdU, γH2AX, and cleaved caspase 3 (CC3) on 7-day recovery pancreata of *Egfr[f/f];Ptf1a[FlpO/+]; R26[CreERT/+]* mice treated with 2 weeks of cerulein followed by vehicle or tamoxifen treatment (n > 3). *Scale bar*: 50 μm. Significance was calculated using an unpaired *t* test. *P < .05, **P < .01.
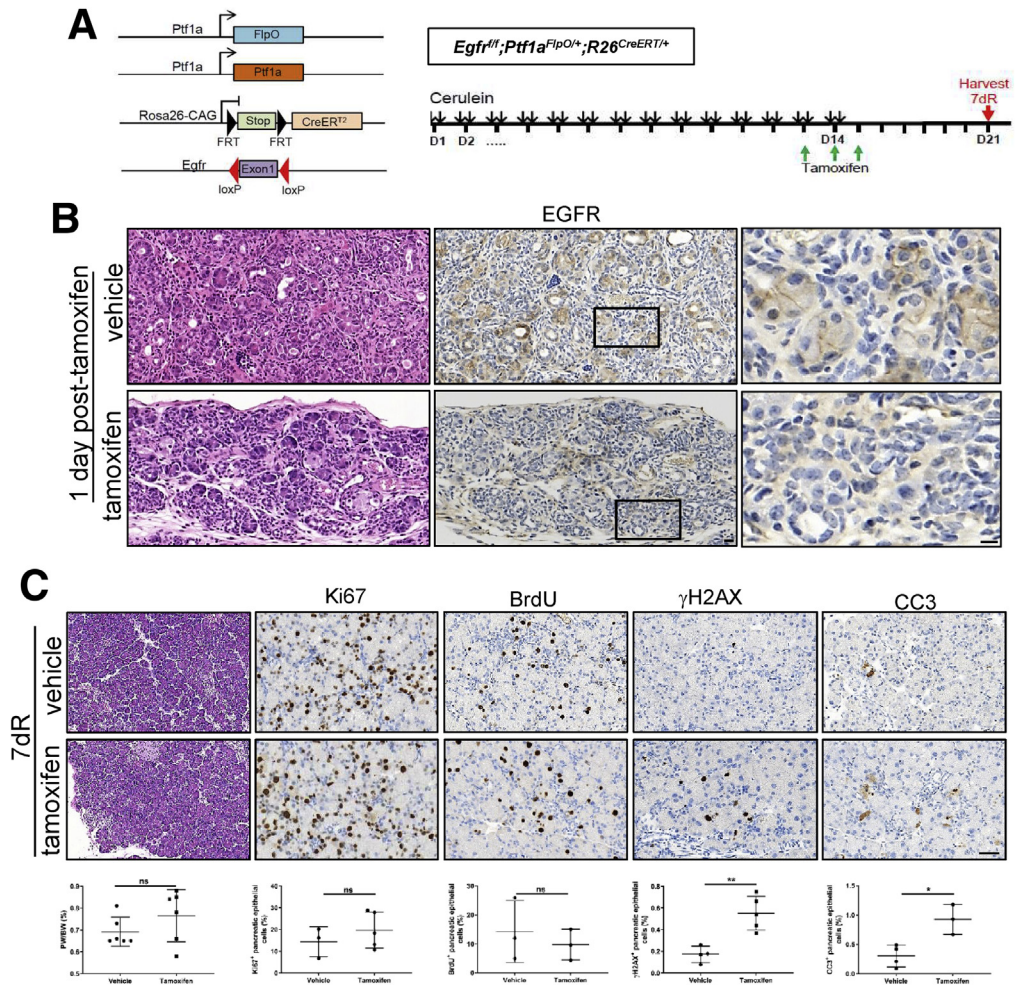
Wild-type C57BL/6 mice and *CD11b-DTR* mice (B6.FVB-471 Tg [ITGAM-DTR/EGFP]34Lan/J) were obtained from Jackson Laboratory (Bar Harbor, ME). The *Hbegf[f/f];LysM-Cre* mouse was generated by crossing the *LysM-Cre*[31] mouse with the *Hbegf[f/f]* mouse[32] (a gift from Dr S. Higashiyama, Ehime University, Ehime, Japan). The *R26[MASTR]* (Rosa26[MASTR[frt-STOP-frt-GFPcre]]) reporter mouse was purchased from Jackson Laboratory.

Egfr[f/f];Ptf1a[FlpO/+];R26[CreERT/+] mice were generated by intercrossing *Egfr[f/f];Ptf1a[FlpO/+]* and *FSF-R26[CAG-CreERT2/+]* animals (a gift from Dieter Saur, Technical University of Munich, Munich, Germany).[46] Mice bearing the *Ptf1a[FlpO]* allele were derived by recombinase-mediated cassette exchange using previously described methods and mouse embryonic stem cells (mESCs) containing a floxed cassette acceptor allele with the *Ptf1a* gene locus (15286998, 18294628).[45,57] Briefly, a *Ptf1a[FlpO(HygroR)]* cassette exchange vector was constructed that replaces *Ptf1a* coding sequences with a *FlpO* coding sequence. FlpO was amplified from pPGKFLPobpA (made by Phil Soriano, obtained from Addgene Watertown, MA).[58] After using the *Ptf1a[FlpO(HygroR)]* exchange to perform recombinase-mediated cassette exchange, cells were screened by polymerase chain reaction (PCR) to identify correctly exchanged clones, and cells from a single selected clone (2F12/2B4) were injected into C57BL/6J blastocysts to generate chimeric mice, which then bred with other C57BL/6J mice to produce *Ptf1a[FlpO]* mice.

Ptf1a[FlpO] mice are genotyped by PCR using the primer pair FLPO327-2F (5'-GGA GTTCACCATCATCCCTTACAACG-3') and FLPO755-R (5'-CTCAGGAACTCGTCCAGGTACA-3').

Experimental pancreatitis was induced, as described previously, by administering 250 μg/kg cerulein (46-1-50; American Peptide Company, Inc, Sunnyvale, CA) intraperitoneally twice daily for 2 weeks in 8-week-old mice[11] For myeloid cell depletion, 25 μg/kg DT (BML-G135-0001; Enzo Life Science, New York, NY) was injected intraperitoneally at day 1 and day 4 after cerulein treatment.[59] For EGFR ablation, mice were gavaged once daily with corn oil (vehicle) or 5 mg tamoxifen (T5648; Sigma-Aldrich, St. Louis, MO) for 3 days. For BrdU (bromodeoxyuridine) incorporation, BrdU (B9285; Sigma-Aldrich) was prepared in saline and 50 mg/kg was injected intraperitoneally 2 hours before euthanasia.

Table 1. Antibodies Used in This Study

Antibody	Company	Catalog no.	Lot no.	
CK19	Developmental Studies Hybridoma Bank (Iowa City, IA)	Troma III		IHC
Amylase	Sigma	A8273	090M4801	IHC
Ki67	Abcam (Cambridge, UK)	ab15580	GR309731-1	IHC, IF
Cleaved caspase 3	Cell Signaling (Danvers, MA)	9664L	21	IHC, IF
γH2AX	Cell Signaling	9718S	13	IHC, IF
γH2AX	Abcam	ab1174	GR3222535-3	WB, IF
F4/80	Bio-Rad (Hercules, CA)	MCA497		IHC
Dimethyl-histone H4	Abcam	ab9052	GR3185175-1	IHC
Dimethyl-histone H4	Cell Signaling	9759S	1	WB, IF
Monomethyl-histone H4	Cell Signaling	9724S	1	WB
53BP1	Novus (Centennial, CO)	NB100304SS	D-9	IF
BrdU	Abcam	ab3626	662915	IHC
CD45	Millipore (Burlington, MA)	05-1416	1975096	IF
GAPDH	Cell Signaling	2118S	10	WB
SOD	Enzon	ADISOD101	1101319	WB
Lamin A/C	Cell Signaling	2032S	6	WB
EGFR	Abcam	ab52894	GR3214138-7	WB, IHC
E-cadherin	Abcam	ab11512	GR155780-1	IF
E-cadherin	BD Pharmingen (San Jose, CA)	610182	8053703	IF
αSMA	Sigma	a2547	084M4795V	IF
GFP	Rockland (Pottstown, PA)	600-406-215	32193	IHC
CD45	Fisher Scientific	MCD4528	1884979	Flow cytometry
CD11b	BD Pharmingen	BDB557657	5351540	Flow cytometry
F4/80	Fisher Scientific	15-4801-82	4316699	Flow cytometry
CD206	BioLegend	141706	B190722	Flow cytometry
TNFα	BD Pharmingen	554418	6209574	Flow cytometry

αSMA, α-smooth muscle actin; GAPDH, glyceraldehyde-3-phosphate dehydrogenase; IF, immunofluorescence; IHC, immunohistochemistry; WB, Western blot.

Immunohistochemistry and Quantification

Pancreata were removed and fixed in Z-fix (NC9050753; Anatech, Ltd, Battle Creek, MI) overnight. Tissues were processed using a Leica ASP300S tissue processor (Buffalo Grove, IL). Paraffin-embedded tissues were sectioned at 4 μm and stained for specific target proteins using the Discovery Ultra XT autostainer (Ventana Medical Systems, Inc, Tucson, AZ) with antibodies as shown in Table 1, and counterstained with Mayer's hematoxylin. H&E staining was performed using Mayer's hematoxylin solution (NC9220898; Sigma-Aldrich) and eosin Y (HT110116; Fisher, Pittsburgh, PA). Picrosirius red staining was performed according to the manufacturer's instructions (Polysciences, Inc, Warrington, PA). Immunohistochemistry slides were scanned on a Pannoramic SCAN scanner (Perkin Elmer, Seattle, WA). Scanned images were quantified using algorithms provided from Halo software (Indica Labs, Corrales, NM).

Immunofluorescence and Quantification

Immunofluorescence performed on frozen sections was described previously.[60] Basically, pancreata were excised and fixed in Z-fix for 3 hours, followed by an overnight float in 30% sucrose. Pancreata were incubated in a 1:1 mixture of 30% sucrose and optimal cutting temperature embedding medium (OCT) for 30 minutes, embedded in OCT, frozen in liquid nitrogen, and stored at -80°C. Tissue sections (7 μm) were permeabilized in 1× phosphate-buffered saline (PBS) supplemented with 0.1% Triton X-100 (T9284; Sigma-Aldrich, St. Louis, MO) for 1 hour and blocked in 1× PBS supplemented with 5% donkey serum and 1% bovine serum albumin for 1 hour. Sections then were incubated with primary antibody diluted in 1× PBS supplemented with 0.1% Triton X-100 and 1% bovine serum albumin overnight at room temperature, followed by 3 washes in 0.1% Triton X-100/PBS for a total of 1 hour. Sections were incubated with secondary antibodies conjugated with Alexa Fluor (Invitrogen, Carlsbad, CA) for 1 hour at room temperature, followed by 3 washes in 0.1% Triton X-100/PBS. Stained slides were rinsed in deionized water and mounted with Prolong Diamond antifade mountant (P36961; Fisher). Images were acquired on a confocal microscope LSM800 (Zeiss, Oberkochen, Germany).

Co-immunofluorescence with Tyramide Signal Amplification (TSA) was performed using the TSA-plus

Table 2. Primers Used in This Study

Gene	Direction	Sequence
Hprt1	Forward	TCAGTCAACGGGGGACATAAA
Hprt1	Reverse	GGGGCTGTACTGCTTAACCAG
Fizz1	Forward	CCTGCTGGGATGACTGCTAC
Fizz1	Reverse	GTCAACGAGTAAGCACAGGC
Argl	Forward	CAGAAGAATGGAAGAGTCAG
Argl	Reverse	CAGATATGCAGGGAGTCACC
Nos2	Forward	GTTCTCAGCCCAACAATACAAGA
Nos2	Reverse	GTGGACGGGTCGATGTCAC
Il12b	Forward	TGGTTTGCCATCGTTTTGCTG
Il12b	Reverse	ACAGGTGAGGTTCACTGTTTCT
Tnfα	Forward	ACGTCGTAGCAAACCACCAA
Tnfα	Reverse	ATAGCAAATCGGCTGACGGT
Hbegf	Forward	TTGTCCGCGTTGGTGACCGG
Hbegf	Reverse	CTTGGGGTGGCCAGGCCTTG
Tgfα	Forward	TGTGGCCCTGGCTGTCCTCA
Tgfα	Reverse	GGCACTGCCAGGGGTGTTGT
Egf	Forward	CAGCGGACCCAACAGCAGCA
Egf	Reverse	GCACTGACCCGAGCTGCAGG
Areg	Forward	GGAGCCGCTGTCGTGTTGCT
Areg	Reverse	GTCCACCGGCACTGTGGTCC
Ereg	Forward	CACTCCGCAAGCTGCACCGA
Ereg	Reverse	TGCACTTGAGCCACACGGGG
Nrg1	Forward	AACAGCAGGCACAGCAGCCC
Nrg1	Reverse	AGGGGAGCTTGGCGTGTGGA
Nrg2	Forward	GGAGATCCAGATGGCAGATTAC
Nrg2	Reverse	GTGAGAAGGTGAACAGGAGTG
Nrg3	Forward	TGCCGAAAACAGACTCCATC
Nrg3	Reverse	CCCACGATGACAATTCCAAAG
Nrg4	Forward	GGACAGAGACAGCCTTAAACAG
Nrg4	Reverse	AAGAATCGGAGAACTGAGCAC

fluorescence evaluation kit (NEL741E001KT; Perkin Elmer) on paraffin-embedded sections for γH2AX and cleaved caspase-3. For quantification of nuclear foci of γH2AX and 53BP1, images were taken by a confocal microscope (LSM800; Zeiss). Four to 6 separated 60× fields (>300 cells) were quantified for each pancreas sample using the find maxima function of ImageJ software (National Institutes of Health, Bethesda, MD). Cells containing γH2AX apoptotic patterns (ring staining, nuclear pan-staining, and pan-staining in apoptotic bodies) were quantified manually on 60× images taken by confocal microscope. The total cell number was counted by HALO (Perkin Elmer, Seattle, WA) software based on Hoechst 33342 staining. CD45$^+$ cells were excluded.

Flow Cytometric Sorting

Preparation of single-cell suspensions of pancreas was performed as previously described.[49] Briefly, pancreata

were minced using a pair of dissecting scissors, followed by digestion in 1 mg/mL collagenase type V (C9263; Sigma) in Hank's balanced salt solution (SH3026801; Fisher) for 15 minutes at 37°C. Cells were washed in Hank's balanced salt solution once, followed by incubation in RBS lysis buffer (420301; Biolegend, San Diego, CA) for 5 minutes. After passing through a 40-μm strainer (22363547; Fisher), single-cell suspensions were incubated with fluorescently conjugated antibodies (as shown in Table 1) diluted in fluorescence-activated cell sorter buffer (2% fetal bovine serum in Hank's balanced salt solution). Cell analysis and sorting was performed using MoFlo Asterio sorter (Beckman Coulter, Indianapolis, IN). Macrophages (CD45$^+$;CD11b$^+$;F4/80$^+$) were sorted and lysed in RLT plus buffer (QIA74136; Qiagen, Valencia, CA) for RNA isolation.

Cell Culture and Treatment

A total of 266.6 cells were purchased from American Type Culture Collection (Manassas, VA) and maintained in Dulbecco's modified Eagle medium (DMEM) containing 10% fetal bovine serum (F2442; Sigma-Aldrich) and 50 ug/mL gentamicin (15710072; Thermo Fisher Scientific, Waltham, MA) in a 37°C incubator with 5% CO_2. H_2O_2 (NDC0869087143; Thermo Fisher Scientific) was used at a final concentration of 500 μmol/L for 1 hour at 37°C. Mouse recombinant HB-EGF (CYT-068; ProSpec, East Brunswick, NJ) was used to treat cells at a final concentration of 100 ng/mL in serum-free DMEM. Transfection of siRNA was performed using the Lipofectamine RNAiMax reagent kit according to the manufacturer's protocol (13778075; Thermo Fisher Scientific). Nontargeting and mouse Egfr siRNAs were purchased from (Dharmacon, Lafayette, CO). After 48 hours of transfection, cells were treated with H_2O_2 for DNA damage response experiments.

Immunoblot Analysis

Cells were lysed in RIPA buffer supplemented with protease inhibitor cocktail (PIA32965; Thermo Fisher Scientific) and PhosSTOP phosphatase inhibitor cocktail (4906845001; Sigma-Aldrich) followed by sonication. Protein concentrations were determined using the BCA Protein Assay Kit (PI23228; Thermo Fisher Scientific). A nuclear-cytoplasmic fraction was made using NE-PER nuclear and cytoplasmic extraction reagents kit (78833; Thermo Fisher Scientific) according to the manufacturer's protocol. Proteins were separated using sodium dodecyl sulfate gel electrophoresis and transferred to a polyvinylidene difluoride membrane (IPVH00010; VWR, Radnor, PA). Primary antibodies are listed in Table 1. Secondary antibody coupled to horseradish peroxidase (GE Healthcare, Pittsburgh, PA) and the enhanced chemiluminescence detection system (Western Pico ECL, Thermo Fisher Scientific) were used to visualize proteins. Quantification of Western blots was performed using ImageJ software.

Comet Assay

DNA breaks were measured using a comet assay, which was performed under alkaline conditions. Single-cell suspensions were processed according to the manufacturer's instructions (4250050-K, CometAssay kit; Trevigen, Gaithersburg, MD). The percentage of DNA in the comet tails was measured using CometScore 2.0 (TriTek Corp, Wilmington, DE).

RNA Isolation and Quantitative PCR

RNA was isolated using an RNeasy Mini kit (QIA74136; Qiagen). The complementary DNA was synthesized by using an iScript complementary DNA synthesis kit (BIO1708891; Bio-Rad, Hercules, CA). Quantitative PCR was performed with Fast SYBR Green (4385612; Thermo Fisher Scientific, Inc) master mix on a Viia7 thermocycler (Life Technologies, Grand Island, NY). The resulting threshold cycle (Ct) obtained from fluorescence was used to find a mean Ct value, and the relative amounts of messenger RNA were determined as $2^{-\Delta Ct}$, where ΔCt is the mean Ct minus the Ct of the housekeeping gene Hprt1. Primer sets used for quantitative PCR are listed in Table 2.

Isolation and Culture of Bone Marrow–Derived Macrophages

Bone marrow cells were isolated from the femurs of 8- to 12-week-old mice. Cells were cultured in DMEM supplemented with 20% fetal bovine serum, 30% L929 conditioned medium, 1 mmol/L sodium pyruvate, and 2.5% penicillin/streptomycin in a 37°C incubator with 5% CO_2 for 5 days. Bone marrow–derived macrophages were polarized with lipopolysaccharide (10 ng/mL) (ALX-581-011-L001; Enzo Life Science) or murine IL4 (10 ng/mL) (214-14; PeproTech, Rocky Hill, NJ) for 24 hours.

Statistical Analysis

Statistics were performed using GraphPad Prism 8.0.2 (San Diego, CA), using an unpaired Student t test for comparison between 2 groups and 1-way or 2-way analysis of variance with multiple comparisons for groups. $P < .05$ was considered statistically significant. ns, no significance.

References

1. Kleeff J, Whitcomb DC, Shimosegawa T, Esposito I, Lerch MM, Gress T, Mayerle J, Drewes AM, Rebours V, Akisik F, Munoz JED, Neoptolemos JP. Chronic pancreatitis. Nat Rev Dis Primers 2017;3:17060.
2. Yadav D, Lowenfels AB. The epidemiology of pancreatitis and pancreatic cancer. Gastroenterology 2013; 144:1252–1261.
3. Machicado JD, Yadav D. Epidemiology of recurrent acute and chronic pancreatitis: similarities and differences. Dig Dis Sci 2017;62:1683–1691.
4. Seifert L, Werba G, Tiwari S, Giao Ly NN, Alothman S, Alqunaibit D, Avanzi A, Barilla R, Daley D, Greco SH, Torres-Hernandez A, Pergamo M, Ochi A, Zambirinis CP, Pansari M, Rendon M, Tippens D, Hundeyin M, Mani VR, Hajdu C, Engle D, Miller G. The necrosome promotes pancreatic oncogenesis via CXCL1 and Mincle-induced immune suppression. Nature 2016;532:245–249.
5. Bockman DE, Boydston WR, Anderson MC. Origin of tubular complexes in human chronic pancreatitis. Am J Surg 1982;144:243–249.
6. Willemer S, Adler G. Histochemical and ultrastructural characteristics of tubular complexes in human acute pancreatitis. Dig Dis Sci 1989;34:46–55.
7. Wagner M, Luhrs H, Kloppel G, Adler G, Schmid RM. Malignant transformation of duct-like cells originating from acini in transforming growth factor transgenic mice. Gastroenterology 1998;115:1254–1262.
8. Habbe N, Shi G, Meguid RA, Fendrich V, Esni F, Chen H, Feldmann G, Stoffers DA, Konieczny SF, Leach SD, Maitra A. Spontaneous induction of murine pancreatic intraepithelial neoplasia (mPanIN) by acinar cell targeting of oncogenic Kras in adult mice. Proc Natl Acad Sci U S A 2008;105:18913–18918.
9. Ardito CM, Gruner BM, Takeuchi KK, Lubeseder-Martellato C, Teichmann N, Mazur PK, Delgiorno KE, Carpenter ES, Halbrook CJ, Hall JC, Pal D, Briel T, Herner A, Trajkovic-Arsic M, Sipos B, Liou GY, Storz P, Murray NR, Threadgill DW, Sibilia M, Washington MK, Wilson CL, Schmid RM, Raines EW, Crawford HC, Siveke JT. EGF receptor is required for KRAS-induced pancreatic tumorigenesis. Cancer Cell 2012;22:304–317.
10. Jensen JN, Cameron E, Garay MV, Starkey TW, Gianani R, Jensen J. Recapitulation of elements of embryonic development in adult mouse pancreatic regeneration. Gastroenterology 2005;128:728–741.
11. Halbrook CJ, Wen HJ, Ruggeri JM, Takeuchi KK, Zhang Y, di Magliano MP, Crawford HC. Mitogen-activated protein kinase kinase activity maintains acinar-to-ductal metaplasia and is required for organ regeneration in pancreatitis. Cell Mol Gastroenterol Hepatol 2017;3:99–118.
12. Jura N, Archer H, Bar-Sagi D. Chronic pancreatitis, pancreatic adenocarcinoma and the black box in-between. Cell Res 2005;15:72–77.
13. Xue J, Sharma V, Habtezion A. Immune cells and immune-based therapy in pancreatitis. Immunol Res 2014;58:378–386.
14. Bhatia M, Brady M, Shokuhi S, Christmas S, Neoptolemos JP, Slavin J. Inflammatory mediators in acute pancreatitis. J Pathol 2000;190:117–125.
15. Shrivastava P, Bhatia M. Essential role of monocytes and macrophages in the progression of acute pancreatitis. World J Gastroenterol 2010;16:3995–4002.
16. Hietaranta A, Mustonen H, Puolakkainen P, Haapiainen R, Kemppainen E. Proinflammatory effects of pancreatic elastase are mediated through TLR4 and NF-kappaB. Biochem Biophys Res Commun 2004; 323:192–196.
17. Gea-Sorli S, Closa D. Role of macrophages in the progression of acute pancreatitis. World J Gastrointest Pharmacol Ther 2010;1:107–111.
18. Liou GY, Doppler H, Necela B, Krishna M, Crawford HC, Raimondo M, Storz P. Macrophage-secreted cytokines drive pancreatic acinar-to-ductal

metaplasia through NF-kappaB and MMPs. J Cell Biol 2013;202:563–577.

19. Xue J, Sharma V, Hsieh MH, Chawla A, Murali R, Pandol SJ, Habtezion A. Alternatively activated macrophages promote pancreatic fibrosis in chronic pancreatitis. Nat Commun 2015;6:7158.

20. Criscimanna A, Coudriet GM, Gittes GK, Piganelli JD, Esni F. Activated macrophages create lineage-specific microenvironments for pancreatic acinar- and beta-cell regeneration in mice. Gastroenterology 2014;147:1106–1118 e11.

21. Besner G, Higashiyama S, Klagsbrun M. Isolation and characterization of a macrophage-derived heparin-binding growth factor. Cell Regul 1990;1:811–819.

22. Ray KC, Moss ME, Franklin JL, Weaver CJ, Higginbotham J, Song Y, Revetta FL, Blaine SA, Bridges LR, Guess KE, Coffey RJ, Crawford HC, Washington MK, Means AL. Heparin-binding epidermal growth factor-like growth factor eliminates constraints on activated Kras to promote rapid onset of pancreatic neoplasia. Oncogene 2014;33:823–831.

23. Taylor SR, Markesbery MG, Harding PA. Heparin-binding epidermal growth factor-like growth factor (HB-EGF) and proteolytic processing by a disintegrin and metalloproteinases (ADAM): a regulator of several pathways. Semin Cell Dev Biol 2014;28:22–30.

24. Iwamoto R, Mekada E. Heparin-binding EGF-like growth factor: a juxtacrine growth factor. Cytokine Growth Factor Rev 2000;11:335–344.

25. Shirakata Y, Kimura R, Nanba D, Iwamoto R, Tokumaru S, Morimoto C, Yokota K, Nakamura M, Sayama K, Mekada E, Higashiyama S, Hashimoto K. Heparin-binding EGF-like growth factor accelerates keratinocyte migration and skin wound healing. J Cell Sci 2005;118:2363–2370.

26. Dao DT, Anez-Bustillos L, Adam RM, Puder M, Bielenberg DR. Heparin-binding epidermal growth factor-like growth factor as a critical mediator of tissue repair and regeneration. Am J Pathol 2018; 188:2446–2456.

27. Duffield JS, Forbes SJ, Constandinou CM, Clay S, Partolina M, Vuthoori S, Wu S, Lang R, Iredale JP. Selective depletion of macrophages reveals distinct, opposing roles during liver injury and repair. J Clin Invest 2005;115:56–65.

28. Saluja AK, Lerch MM, Phillips PA, Dudeja V. Why does pancreatic overstimulation cause pancreatitis? Annu Rev Physiol 2007;69:249–269.

29. Navas C, Hernandez-Porras I, Schuhmacher AJ, Sibilia M, Guerra C, Barbacid M. EGF receptor signaling is essential for k-ras oncogene-driven pancreatic ductal adenocarcinoma. Cancer Cell 2012;22:318–330.

30. Zhang Y, Yan W, Mathew E, Kane KT, Brannon A, Adoumie M, Vinta A, Crawford HC, Pasca di Magliano M. Epithelial-myeloid cell crosstalk regulates acinar cell plasticity and pancreatic remodeling in mice. Elife 2017;6.

31. Clausen BE, Burkhardt C, Reith W, Renkawitz R, Forster I. Conditional gene targeting in macrophages and granulocytes using LysMcre mice. Transgenic Res 1999; 8:265–277.

32. Iwamoto R, Yamazaki S, Asakura M, Takashima S, Hasuwa H, Miyado K, Adachi S, Kitakaze M, Hashimoto K, Raab G, Nanba D, Higashiyama S, Hori M, Klagsbrun M, Mekada E. Heparin-binding EGF-like growth factor and ErbB signaling is essential for heart function. Proc Natl Acad Sci U S A 2003;100:3221–3226.

33. Lonkar P, Dedon PC. Reactive species and DNA damage in chronic inflammation: reconciling chemical mechanisms and biological fates. Int J Cancer 2011; 128:1999–2009.

34. Orosz Z, Csiszar A, Labinskyy N, Smith K, Kaminski PM, Ferdinandy P, Wolin MS, Rivera A, Ungvari Z. Cigarette smoke-induced proinflammatory alterations in the endothelial phenotype: role of NAD(P)H oxidase activation. Am J Physiol Heart Circ Physiol 2007; 292:H130–H139.

35. Ji C. Mechanisms of alcohol-induced endoplasmic reticulum stress and organ injuries. Biochem Res Int 2012; 2012:216450.

36. Geiger-Maor A, Guedj A, Even-Ram S, Smith Y, Galun E, Rachmilewitz J. Macrophages regulate the systemic response to DNA damage by a cell nonautonomous mechanism. Cancer Res 2015;75:2663–2673.

37. Sharma A, Singh K, Almasan A. Histone H2AX phosphorylation: a marker for DNA damage. Methods Mol Biol 2012;920:613–626.

38. Solier S, Pommier Y. The nuclear gamma-H2AX apoptotic ring: implications for cancers and autoimmune diseases. Cell Mol Life Sci 2014;71:2289–2297.

39. Yang H, Mizzen CA. The multiple facets of histone H4-lysine 20 methylation. Biochem Cell Biol 2009; 87:151–161.

40. Chou RH, Wang YN, Hsieh YH, Li LY, Xia W, Chang WC, Chang LC, Cheng CC, Lai CC, Hsu JL, Chang WJ, Chiang SY, Lee HJ, Liao HW, Chuang PH, Chen HY, Wang HL, Kuo SC, Chen CH, Yu YL, Hung MC. EGFR modulates DNA synthesis and repair through Tyr phosphorylation of histone H4. Dev Cell 2014;30:224–237.

41. Korotkevych NV, Labyntsev AJ, Kolybo DV, Komisarenko SV. The soluble heparin-binding EGF-like growth factor stimulates EGF receptor trafficking to the nucleus. PLoS One 2015;10:e0127887.

42. Collins AR. The comet assay for DNA damage and repair: principles, applications, and limitations. Mol Biotechnol 2004;26:249–261.

43. Alwan HA, van Zoelen EJ, van Leeuwen JE. Ligand-induced lysosomal epidermal growth factor receptor (EGFR) degradation is preceded by proteasome-dependent EGFR de-ubiquitination. J Biol Chem 2003; 278:35781–35790.

44. Panier S, Boulton SJ. Double-strand break repair: 53BP1 comes into focus. Nat Rev Mol Cell Biol 2014;15:7–18.

45. Kawaguchi Y, Cooper B, Gannon M, Ray M, MacDonald RJ, Wright CV. The role of the transcriptional regulator Ptf1a in converting intestinal to pancreatic progenitors. Nat Genet 2002;32:128–134.

46. Schonhuber N, Seidler B, Schuck K, Veltkamp C, Schachtler C, Zukowska M, Eser S, Feyerabend TB, Paul MC, Eser P, Klein S, Lowy AM, Banerjee R, Yang F, Lee CL, Moding EJ, Kirsch DG, Scheideler A, Alessi DR,

Varela I, Bradley A, Kind A, Schnieke AE, Rodewald HR, Rad R, Schmid RM, Schneider G, Saur D. A next-generation dual-recombinase system for time- and host-specific targeting of pancreatic cancer. Nat Med 2014; 20:1340–1347.

47. Siveke JT, Lubeseder-Martellato C, Lee M, Mazur PK, Nakhai H, Radtke F, Schmid RM. Notch signaling is required for exocrine regeneration after acute pancreatitis. Gastroenterology 2008;134:544–555.

48. Fendrich V, Esni F, Garay MV, Feldmann G, Habbe N, Jensen JN, Dor Y, Stoffers D, Jensen J, Leach SD, Maitra A. Hedgehog signaling is required for effective regeneration of exocrine pancreas. Gastroenterology 2008;135:621–631.

49. Zhang Y, Yan W, Collins MA, Bednar F, Rakshit S, Zetter BR, Stanger BZ, Chung I, Rhim AD, di Magliano MP. Interleukin-6 is required for pancreatic cancer progression by promoting MAPK signaling activation and oxidative stress resistance. Cancer Res 2013;73:6359–6374.

50. Shaltiel IA, Krenning L, Bruinsma W, Medema RH. The same, only different - DNA damage checkpoints and their reversal throughout the cell cycle. J Cell Sci 2015; 128:607–620.

51. van Nuland R, Gozani O. Histone H4 lysine 20 (H4K20) methylation, expanding the signaling potential of the proteome one methyl moiety at a time. Mol Cell Proteomics 2016;15:755–764.

52. Jorgensen S, Schotta G, Sorensen CS. Histone H4 lysine 20 methylation: key player in epigenetic regulation of genomic integrity. Nucleic Acids Res 2013; 41:2797–2806.

53. Kawanishi S, Ohnishi S, Ma N, Hiraku Y, Murata M. Crosstalk between DNA damage and inflammation in the multiple steps of carcinogenesis. Int J Mol Sci 2017;18.

54. Yu JH, Lim JW, Kim KH, Morio T, Kim H. NADPH oxidase and apoptosis in cerulein-stimulated pancreatic acinar AR42J cells. Free Radic Biol Med 2005;39:590–602.

55. Mitamura T, Higashiyama S, Taniguchi N, Klagsbrun M, Mekada E. Diphtheria toxin binds to the epidermal growth factor (EGF)-like domain of human heparin-binding EGF-like growth factor/diphtheria toxin receptor and inhibits specifically its mitogenic activity. J Biol Chem 1995;270:1015–1019.

56. Collins MA, Bednar F, Zhang Y, Brisset JC, Galban S, Galban CJ, Rakshit S, Flannagan KS, Adsay NV, Pasca di Magliano M. Oncogenic Kras is required for both the initiation and maintenance of pancreatic cancer in mice. J Clin Invest 2012;122:639–653.

57. Burlison JS, Long Q, Fujitani Y, Wright CV, Magnuson MA. Pdx-1 and Ptf1a concurrently determine fate specification of pancreatic multipotent progenitor cells. Dev Biol 2008;316:74–86.

58. Raymond CS, Soriano P. High-efficiency FLP and PhiC31 site-specific recombination in mammalian cells. PLoS One 2007;2:e162.

59. Zhang Y, Velez-Delgado A, Mathew E, Li D, Mendez FM, Flannagan K, Rhim AD, Simeone DM, Beatty GL, Pasca di Magliano M. Myeloid cells are required for PD-1/PD-L1 checkpoint activation and the establishment of an immunosuppressive environment in pancreatic cancer. Gut 2017;66:124–136.

60. Delgiorno KE, Hall JC, Takeuchi KK, Pan FC, Halbrook CJ, Washington MK, Olive KP, Spence JR, Sipos B, Wright CV, Wells JM, Crawford HC. Identification and manipulation of biliary metaplasia in pancreatic tumors. Gastroenterology 2014; 146:233–244 e5.

Correspondence
Address correspondence to: Howard Crawford, PhD, University of Michigan, 4304 Rogel Cancer Center, 1500 East Medical Center Drive, SPC 5936, Ann Arbor, Michigan 48109-5936. e-mail: howcraw@umich.edu; fax: (734) 647–9654.